THEORY, DEVELOPMENT AND TESTING OF AN ICE-OIL BOOM

by
Gee Tsang[1] and Nick Vanderkooy[2]

[1]Hydraulics Research Division
[2]Environmental Protection Service
Canada Centre for Inland Waters
Burlington, Ontario
November 1978

THEORY, DEVELOPMENT AND TESTING OF AN ICE-OIL BOOM

by

Gee Tsang[1] and Nick Vanderkooy[2]

EPS Publication No.
November 1978

1 Research Scientist, Hydraulics Research Division, National Water Research Institute, CCIW, Burlington, Ontario

2 Manager, Ontario Region, Environmental Emergency Branch, Environmental Protection Service

TABLE OF CONTENTS

LIST OF FIGURES

LIST OF TABLES

ABSTRACT

This paper reports the development of a novel boom for use when oil is spilled on flowing water infested with ice floes. The boom utilizes the ruddering principle and consists of a perforated boom body and a number of fins behind the boom. The angle between the fins and the boom is adjustable. The impinging of the current on the fins brings the boom into the flow and the boom makes an angle with the current. While the surface current and the oil slick are able to pass through the perforating holes in the boom to the ice-free area behind the boom, the ice floes are barred from entering the area and are guided to one side. After flowing through the perforated holes, the surface current is further deflected by the fins towards the shore, carrying with it the oil slick to the slow shore region for easy recovery.

Detailed theoretical analysis is made relating the angle between the fins and the boom to the angle between the boom and the current; relating the size of the ice floe that a boom can deflect to the corresponding yielding angle of the boom and relating the force on the boom to the angle between the fins and the boom. Different parameters are identified and their effects on the performance of the boom are thoroughly studied. Based on the theoretical investigations, one now can design a boom for practical use.

Preliminary laboratory experiments were performed on a model boom. The laboratory testing confirmed the feasibility of the ice-oil boom.

A prototype boom was constructed and field tested in the Detroit River. The field experiment confirmed theoretical predictions and showed that the newly developed boom can perform its duties as expected.

Further laboratory experiments are being planned for obtaining some design coefficients. A second generation boom will also be constructed and tested aiming to improve the deployment procedure and the performance of the boom.

1.0 INTRODUCTION

When oil is spilled in rivers with drifting ice floes, the conventional containment booms and recovery apparatus have great difficulty in performing their functions. The ice floes will rip the conventional booms apart and jam the intakes of the recovery machinery. In fact, even the operation of small crafts in a fast current with drifting ice floes is not an easy task. The small vessels can capsize easily when rammed by large ice floes.

The presence of ice floes in rivers during winter months is not uncommon and is not necessarily confined to spring breakup months. Statistical analysis of the ice conditions in Detroit and St. Clair rivers, for instance, showed that the most likely form of ice in the two rivers is ice floes (Tsang, 1975). An aerial survey by Tsang made in the winter of 1974 showed that most ice floes were less than the size of a tennis court. However, occasionally large floes spanning up to half the river's width would drift down the two rivers.

To contain and recover oil in an ice infested river, an ice free area has to be created first where conventional clean up gear may be employed. Such an area is obtained if a barrier can be set up which, while permitting the oil slick to pass through, will bar ice floes from entering the area.

In the above quoted work by Tsang studying how to contain and recover spilled oil on the Detroit and St. Clair rivers in winter should such an oil spill occur, Tsang proposed the use of perforated booms at an angle to the flow. While the slick should have little difficulty in passing through the boom through the openings provided, the ice floes would be guided by the boom and deflected to one side.

There is enough evidence showing that, even under ice free conditions, the containment of oil by conventional booms on fast flowing water is ineffective (Vanderkooy et al, 1976; Foley and Tresidder, 1977). It will be desirable, therefore, if the perforated boom proposed above can direct the oil slick to the slow shore region for containment and recovery, in addition to barring the ice floes.

Not only are conventional booms ineffective in containing oil on fast flowing water, but their deployment in fast current is also difficult because they need to be anchored by the two ends, many times with intermediate anchoring points in between. For easy deployment, therefore, if an ice barring boom is to be deployed, it will be highly desirable if the boom only needs to be anchored at one point, preferably from the shore.

Glance booms have long been used by the pulp and paper industry to confine the pulp wood to the desired channel (Koroleff, 1932; Lazier, 1964). Figure 1 shows the configuration of a glance boom. It is seen from Figure 1 that the boom needs only to be moored by its upstream end from the shore. The fins or rudders, when impinged on by the flow, will take the boom into the current. By varying the angle between the fins and the boom, the angle between the boom and the current can be changed. The oncoming pulp wood, upon meeting the boom, is guided to one side.

An ice infested river is similar to a river transporting pulp wood. A glance boom, therefore, may be used as an ice barring barrier. If perforated openings are provided to the boom, then the oil slick will be able to flow through them to the ice-free area behind. The surface current, after flowing through the openings, will impinge on the fins and be deflected towards the shore. The shoreward current will carry the oil slick to the slow shore region for easy containment and recovery. According to the above, it appears, a perforated glance boom is the ice-oil boom that one is looking for.

The envisaged boom shown above also has the very desirable built-in stress-relief characteristic. Should the boom be hit by an extraordinarily large ice floe, it will simply yield by swinging towards the shore instead of failing. Once the ice floe is passed, the boom will swing back into the current again.

It is worth mentioning that the glance boom also inspired the development of boom deflectors by Brodsky et al (1977). The deflectors are in the form of individual fins that can be clipped onto conventional booms. The clipping of deflectors to a boom makes the boom a straight deflection boom that only needs to be moored by its upstream end. Upon meeting the boom, the oil slick is guided to the desirable point for recovery.

Deflecting the oil slick towards the shore region by deflection of the surface current has also been contemplated by Eryuzlu and Hausser (1977). They proposed to deflect the surface layer of a river by a set of current deflectors. The deflectors are in the form of floating aerofoils and are deployed like flying kites in the horizontal plane. When placed in water at the shore, the current will take the deflectors into the flow. At the equilibrium position, the deflectors deflect the impinging current towards the shore, carrying the oil slick with it. A model study of the deflectors simulating the St. Lawrence River situation showed that several metres of the surface layer should be deflected. This calls for the construction of massive deflectors and mooring structures.

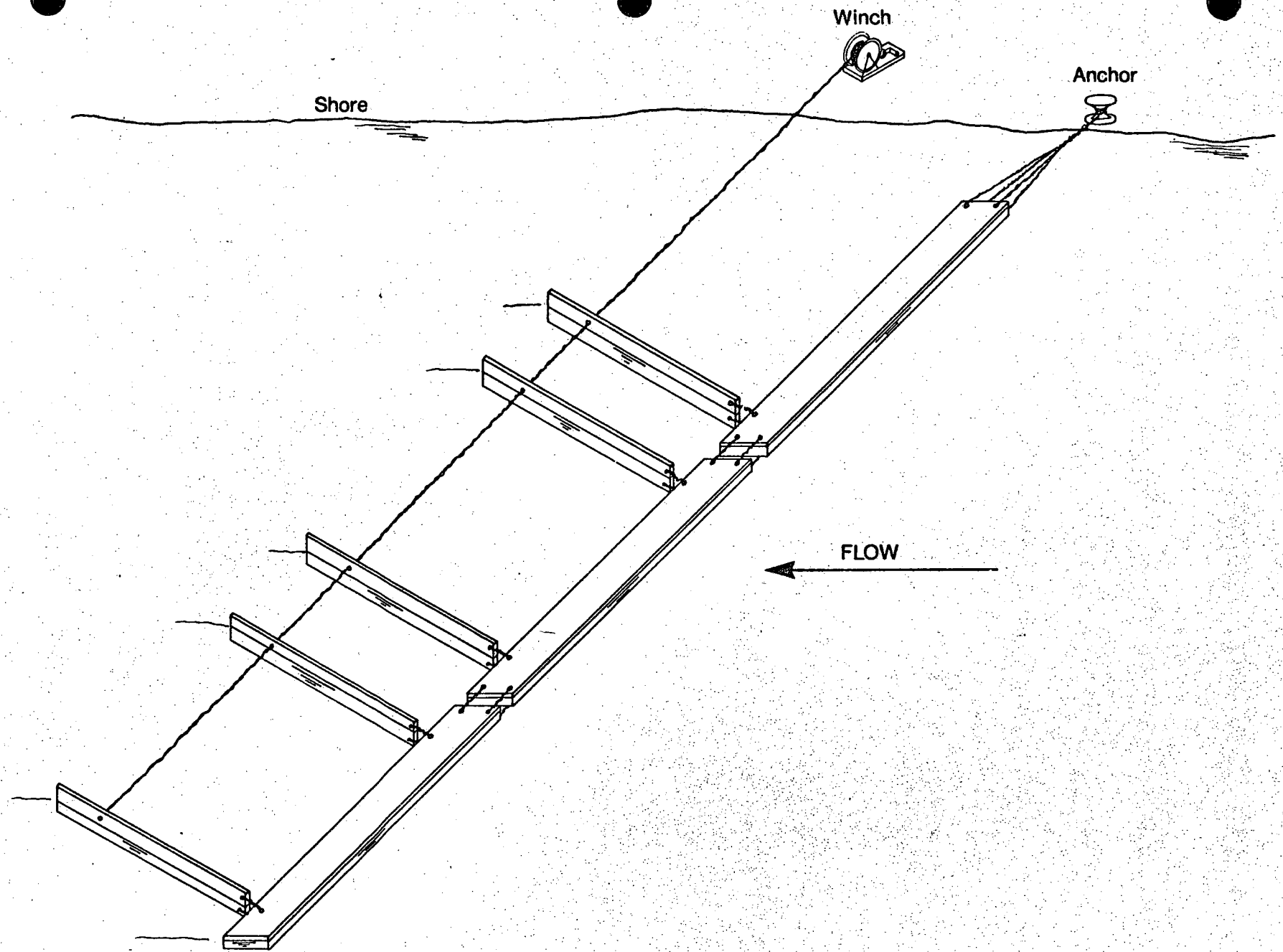

Fig.1 Configuration of a glance boom (as shown by Koroleff and Lazier)

Although the glance boom has been used for many years, it has not been comprehensively analysed. In this paper, the proposed ice-oil boom will first be theoretically analysed in detail. Then, the field test of a prototype boom, which was designed and constructed based on preliminary theoretical investigations and model testings, will be reported. The experimental findings are compared with theoretical predictions and recommendations are drawn for further development of the boom.

2.0 THEORY

The glance booms used by the timber industry are made up of individual units as shown in Figure 1. The units are linked together either with ropes or shackles. While such a flexible boom may be adequate in deflecting pulp wood, both laboratory and field tests showed that it deforms excessively when hit by ice floes of relatively large size and thus is unacceptable. The ice-oil boom to be developed, therefore, should be rigidly connected between units.

Figure 2 shows a rigidly constructed boom of N units. For each unit, it comprises a section of the boom body of length L_b and a fin of length L_f. The fin is hinged to the boom section at a distance L_a from the upstream end of the section and L_g indicates the gap between the fin and the boom for reducing turbulence. The upstream, unfinned part is for protecting the fins from ice damages and was found to be necessary from the field experiment. The following analyses are made on such a boom.

2.1 Moments Acting on the Boom

Figure 2 shows the envisaged ice-oil boom being deflected by the current to the left. The diagram shows that when the fin angle is α, the equilibrium boom angle is θ.

In the analysis here, the following assumptions are used:

(i) The drags on the boom and on the fins are produced by the normal component of the velocity alone.

(ii) For each unit, the boom drag acts on the mid point of the boom section and the fin drag acts on the mid point of the fin.

(iii) The presence of the fins does not affect the hydraulic behaviour of the boom, and vice versa.

According to the above assumptions, the moment due to the drag on the boom section of the nth unit about the upstream end of the boom point A is seen to be

$$m_{bn} = \left(\frac{1}{2} C_D \rho V^2 \sin^2 \theta A_b\right) L_b \left(\frac{L_u}{L_b} + n - \frac{1}{2}\right) \qquad (1)$$

where C_D is the drag coefficient, ρ is the density of water, V is the flow velocity, A_b is the projected area of the boom section to the normal velocity component

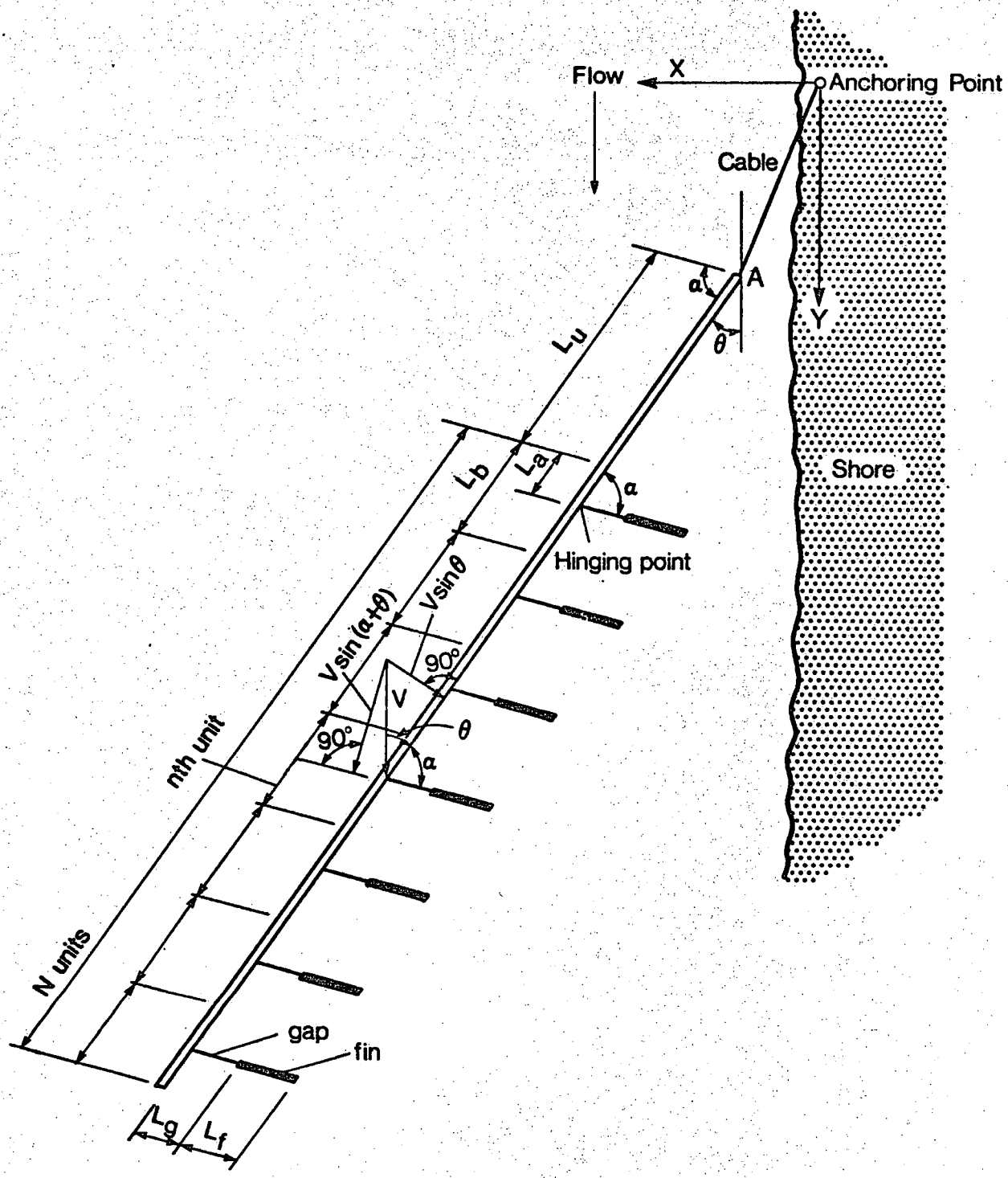

Fig 2 Definition diagram of ice-oil boom

and the first bracket in the equation is the drag on the boom section. For all other units, similar equations can be written. The summation of all the N moments gives

$$\sum_{n=1}^{N} m_{bn} = \frac{1}{2} C_D \rho V^2 \sin^2 \theta A_b L_b \left(\frac{L_u}{L_b} + \frac{N}{2} \right) N \qquad (2)$$

For the upstream protective part L_u, the moment by the drag on it about A is

$$m_{bu} = \frac{1}{2} C_D \rho V^2 \sin^2 \theta A_b L_b \left(\frac{1}{2} \frac{A_u L_u}{A_b L_b} \right) \qquad (3)$$

where A_u is the projected area of it to the normal velocity component. The summation of Equations 2 and 3 gives the total moment on the boom body about A M_b. If M_b is normalized by the following equation

$$M_{b_*} = \frac{M_b}{\frac{1}{2} C_D \rho V^2 A_b L_b} \qquad (4)$$

it can be shown that

$$M_{b_*} = \sin^2 \theta \left[\frac{L_u}{L_b} \left(\frac{1}{2} \frac{A_u}{A_b} + N \right) + \frac{N^2}{2} \right] \qquad (5)$$

According to the theory of mechanics, the moment by the drag on the fin of the nth unit about point A is given by

$$\begin{aligned} m_{fn} = &- \left[\frac{1}{2} C_D \rho V^2 \sin^2 (\alpha+\theta) A_f \right] (L_g + \frac{1}{2} L_f) \\ &+ \left[\frac{1}{2} C_D \rho V^2 \sin^2 (\alpha + \theta) A_f \right] (L_u + (n-1) L_b + L_a) \cos \alpha \end{aligned} \qquad (6)$$

where A_f is the immersed area of the fin. The quantity inside the square bracket is the drag on the fin. The first term on the right side of the equation is the clockwise moment by the drag on the fin about the hinging point and the second term is the counterclockwise moment of the drag force, now considered to be acting on the hinging point, about point A. Again, similar expressions may be written for all the N fins. The summation of all the moments and the subsequent normalization of the resultant moment by the denominator of Equation 4 give the following non-dimensional moment by the drags on the fins of the boom:

$$M_{f_*} = \text{Sin}^2(\alpha+\theta)\frac{A_f}{A_b}N\left[\left(\frac{L_u}{L_b}+\frac{L_a}{L_b}+\frac{N-1}{2}\right)\text{Cos}\,\alpha-\left(\frac{L_g}{L_b}+\frac{L_f}{2L_b}\right)\right] \quad (7)$$

Equations 5 and 7 are derived when the boom is deflected by the current to the left. Under certain parametric conditions, it is possible for the boom to be deflected by the current to the right. In such a case, two similar equations may be derived. If the boom angle is considered to be positive when the boom is deflected to the left by the current and negative when the boom is deflected to the right, these two equations may be absorbed into Equations 5 and 7 and one has

$$M_{b_*} = \pm\,\text{Sin}^2(\pm\theta)\left[\frac{L_u}{L_b}\left(\frac{1}{2}\frac{A_u}{A_b}+N\right)+\frac{N^2}{2}\right] \quad (8)$$

$$M_{f_*} = \text{Sin}^2(\alpha+\theta)\frac{A_f}{A_b}N\left[\left(\frac{L_u}{L_b}+\frac{L_a}{L_b}+\frac{N-1}{2}\right)\text{Cos}\,\alpha-\left(\frac{L_g}{L_b}+\frac{L_f}{2L_b}\right)\right] \quad (9)$$

For equation 8, the positive and negative signs are used when the boom angle is positive and negative respectively. In the equation, $\text{Sin}^2(\pm\theta)$ is not written as $\text{Sin}^2\theta$ as not to mask its mathematical true form for later mathematical operations.

2.2 Effect of positioning of Hinging Point of Fin

The ice-oil boom is intended to deflect ice floes and thus should be deflected to the left by the current for shielding the fins behind the boom. For practical engineering construction, the upstream protective part should be formed by one or more boom units without the fins and this makes $A_u/A_b=L_u/L_b$. Under the above conditions, Equation 8 has the form of

$$M_{b_*} = \text{Sin}^2\theta\left[\frac{L_u}{L_b}\left(\frac{1}{2}\frac{L_u}{L_b}+N\right)+\frac{N^2}{2}\right] \quad (10)$$

The above moment is always positive for reducing the boom angle θ and is independent of the fin angle α.

As to the fin moment M_{f_*}, it is seen from Equation 9 and with reference to Figure 2 that M_{f_*} consists of two parts. The first part is for reducing the boom angle θ when $\alpha < 90^\circ$ (counterclockwise moment) and increasing θ when $\alpha\ 90^\circ$ (clockwise moment) while the second part is always for increasing the boom angle

θ (clockwise moment). Since the ice-oil boom is for barring ice floes, it should be made to swing into the current as much as possible. The fin angle of the boom α under working conditions, therefore, should be greater than 90^{o}.

When $\alpha > 90^{o}$, it is seen from Equation 9 that the moment for increasing θ increases with L_a/L_b. To obtain the maximum clockwise moment, L_a/L_b, therefore, should be assigned the maximum value of unity. L_a/L_b equals unity requires that the hinging point of the fin be placed at the end of the unit.

2.3 Criteria for Direction of Boom Deflection

At equilibrium, under ice free conditions, one has

$$M_{b_*} + M_{f_*} = 0 \tag{11}$$

The substitution of Equations 8 and 9 to the above equation, under the condition of $L_a/L_b=1$, leads to

$$\begin{aligned} &\mathrm{Sin}^2(\pm\theta)\left[\frac{L_u}{L_b}\left(\frac{1}{2}\frac{L_u}{L_b}+N\right)+\frac{N^2}{2}\right] \\ &= \mathrm{Sin}^2(\alpha+\theta)\,\frac{A_f}{A_b}N\left[\pm\left(\frac{L_g}{L_b}+\frac{L_f}{2L_b}\right)\mp\left(\frac{L_u}{L_b}+\frac{N+1}{2}\right)\mathrm{Cos}\,\alpha\right] \end{aligned} \tag{12}$$

using the upper signs when $\theta > 0$ and using the lower signs when $\theta < 0$.

It is seen from Equation 12 that since the left hand side of the equation is always positive and the quantity outside the bracket on the right hand side of the equation is also positive, one should have

$$\left[\left(\frac{L_g}{L_b}+\frac{L_f}{2L_b}\right)-\left(\frac{L_u}{L_b}+\frac{N+1}{2}\right)\cos\alpha\right] > 0;\ \text{for } \theta > 0 \tag{13}$$

and

$$\left[-\left(\frac{L_g}{L_b}+\frac{L_f}{2L_b}\right)+\left(\frac{L_u}{L_b}+\frac{N+1}{2}\right)\cos\alpha\right] > 0;\ \text{for } \theta > 0 \tag{14}$$

The above inequalities may be rewritten as

$$\mathrm{Cos}\,\alpha < \frac{\dfrac{L_g}{L_b}+\dfrac{L_f}{2L_b}}{\dfrac{L_u}{L_b}+\dfrac{N+1}{2}};\ \text{for } \theta > 0 \tag{15}$$

and

$$\text{Cos}\,\alpha > \frac{\frac{L_g}{L_b} + \frac{L_f}{2L_b}}{\frac{L_u}{L_b} + \frac{N+1}{2}} \quad ; \text{for } \theta < 0 \tag{16}$$

The above inequalities give the criteria of the fin angle α for the boom to be deflected by the current to the left and to the right.

Since α can never be greater than unity, Equation 16 can never be satisfied when

$$\frac{L_g}{L_b} + \frac{2L_f}{2L_b} > \frac{L_u}{L_b} + \frac{N+1}{2} \tag{17}$$

In other words, under conditions shown by the above inequality, a boom can only be deflected by the current to the left.

2.4 θ-α Relationship under Ice Free Conditions

By rearranging Equation 12 and based on the discussions in the last section, one obtains

$$\theta = \pm\text{Cot}^{-1}\left\{ \frac{1}{\text{Sin}\,\alpha} \left[\frac{\frac{L_u}{L_b}\left(\frac{1}{2}\frac{L_u}{L_b} + N\right) + \frac{N^2}{2}}{\frac{A_f}{A_b} N \left[\pm\left(\frac{L_g}{L_b} + \frac{L_f}{2L_b}\right) \mp \left(\frac{L_u}{L_b} + \frac{N+1}{2}\right) \text{Cos}\,\alpha \right]} \right]^{\frac{1}{2}} - \text{Cot}\,\alpha \right\} \tag{18}$$

using the upper signs when Equation 15 is satisfied and using the lower signs when Equation 16 is satisfied. Based on the above equation, curves of θ versus α may be calculated and plotted.

Equation 18 contains L_u/L_b, N, L_g/L_b, A_f/A_b and L_f/L_b five parameters. To study the effects of these parameters on the θ versue α curve, the different parametric values as shown in Table 1 are used. In the table, the underlined values are for the parameters of a reference curve and are selected as being engineeringly reasonable. To study the effect of a parameter, the different values of that parameter as shown in Table 1 are used one by one while the other parameters remain those of the reference case. The comparison of the different curves so generated reveals the effect of the parameter.

The parameter A_f/A_b may be replaced by $(H_f/H_b)(L_f/L_b)$, where H_f is the depth of the fin in water and H_b is the equivalent depth of the boom in water. Because openings are provided in the boom, H_b will be less than the actual depth of immergence of the boom in water. Since L_f/L_b is already a parameter, H_f/H_b, therefore, may be considered as the parameter replacing A_f/A_b. The values of H_f/H_b, when it is used instead of A_f/A_b, are also shown on Table 1.

TABLE 1 PARAMETRIC VALUES USED IN COMPARATIVE STUDY

L_u/L_b	0	1	2	3	4	5		
N	2	4	6	8	10	12	15	20
L_g/L_b	0	0.1	0.2	0.3	0.4	0.5	1.0	
L_f/L_b	0.5	0.8	1.2	1.4	1.6			
A_f/A_b	0.5	0.8	1.0	1.2	1.4	1.6		
H_f/H_b	1.0	1.2	1.4	1.6	1.8	2.0		

Based on Equation 18 and the parametric values shown in Table 1, different sets of θ versus α curves for different parametric conditions are calculated and plotted as shown in Figure 3 to 8.

Figure 3 shows θ versus α curves of different L_u/L_b values. It is seen from Figure 3 that the curves are of the same shape in the form of a fallen S. From the curves, one sees that a boom under the given parametric conditions will be in the direction of the flow when the fins are completely open at 180°. As the fins are gradually closed, the boom begins to swing to the left into the flow until a maximum boom angle is reached. Thereafter, further closing the fins will reduce the boom angle until $\theta=0$. From that point on, the boom will swing to the other side. It is interesting to see from the curves that the boom will also swing to a maximum angle to the right before swinging back. When the fins are completely closed, the boom will be again in the direction of the flow.

Figure 3 shows that the curves are close together and the value of θ_{max} are greater for booms with smaller L_u/L_b values. This means that, although the increase of the upstream protective part of the boom L_u tends to reduce the maximum angle the boom made with the current, for the shown parametric range at least, such an effect is small and insignificant. For a boom with a protective length five times the unit length, the maximum boom angle is about 24^o and for a boom without the protective part, the maximum obtainable boom angle is only about two degrees greater.

Figure 4 shows θ-α curves of different N values. It is seen from Figure 4 that the curves are of the same form as those in Figure 3, although they diverse more from each other. However, the diversion of the curves is mainly for their lower parts. For the practically important range between $\alpha=180^o$ and the point of maximum boom angle, the curves are almost coincident. Thus, one may conclude that under the present parametric conditions, at least, the number of units used in a boom has little effect on the hydraulic performance of the boom.

In Figure 5 are θ-α curves of different L_g/L_b ratios. These curves are again of the same form as those in Figures 3 and 4. It is seen from Figure 5 that, although curves of higher L_g/L_b values show greater θ_{max} values, the difference in θ_{max} in the selected L_g/L_b range is not much; comes to only about 3^o. For the important range in practice between $\theta=180^o$ and θ_{max}, the curves are almost coincident. Based on Figure 5, one thus sees that increasing the distance between the fins and the boom is not an effective way to increase the boom angle with the flow.

Figure 6 and Figure 7 show the same parametric effect but denote it differently. In Figure 6, the area ratio A_f/A_b is used and in Figure 7, the depth ratio H_f/H_b is employed. Both diagrams are subject to the same constraint of constant length ratio of $L_f/L_b=0.8$.

It is seen from Figure 6 and 7 that with the length of the fins maintained unchanged, the area or the depth of the fins has a great effect on the hydraulic characteristic of the boom. For instance, it is seen from the curves that when the area or the depth of the fins is doubled, the maximum boom angle is increased by close to 7^o. From the lower half of the curves, one sees that when the fin area (or the fin depth) is greater than a certain critical value, there will not be a maximum swinging angle of the boom to the right (θ_{min}). In such cases, the boom will swing continuously in the counterclockwise direction as the fins are further closed.

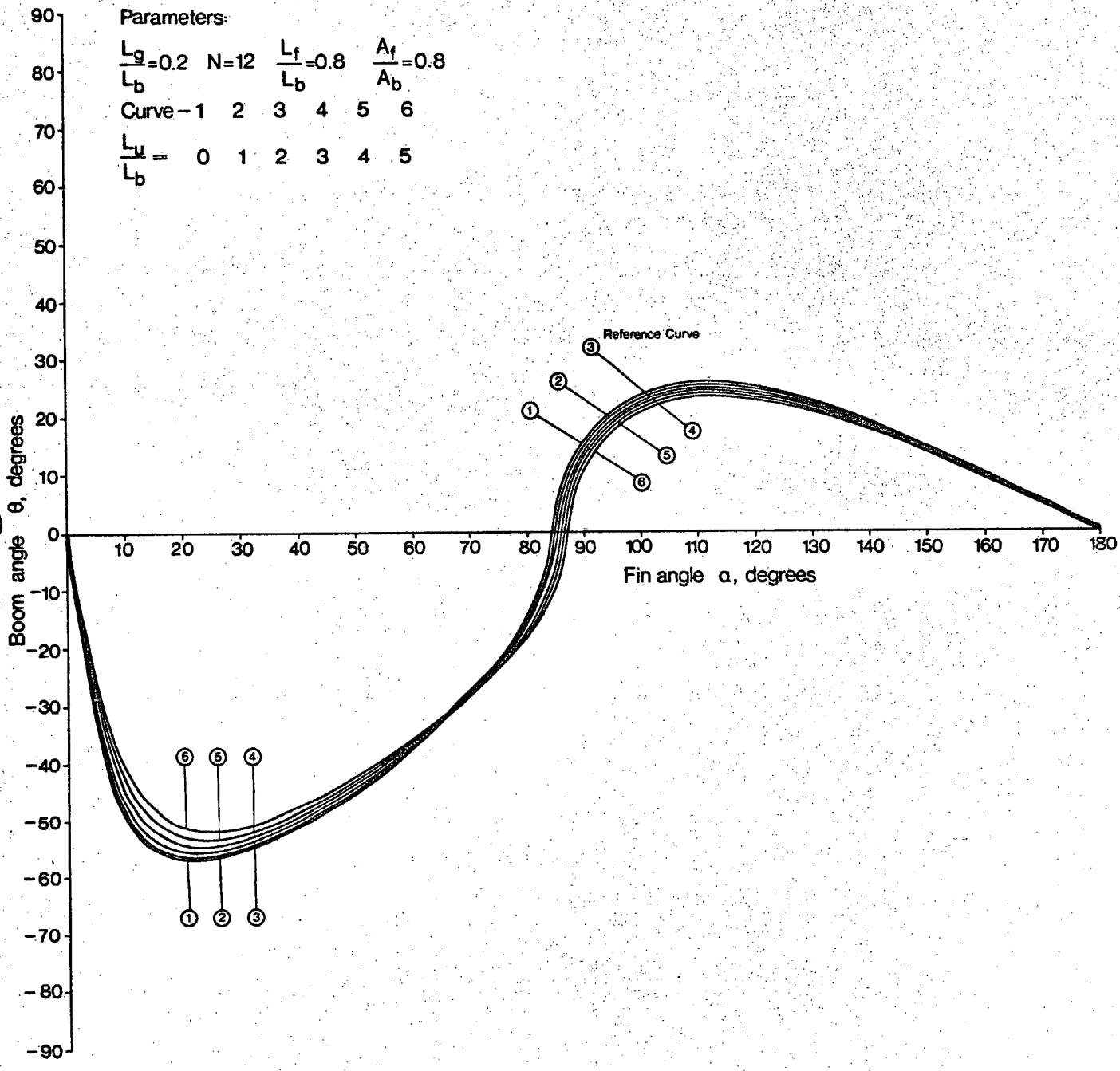

Fig. 3 Boom angle and fin angle relationship for different upstream protective lengths

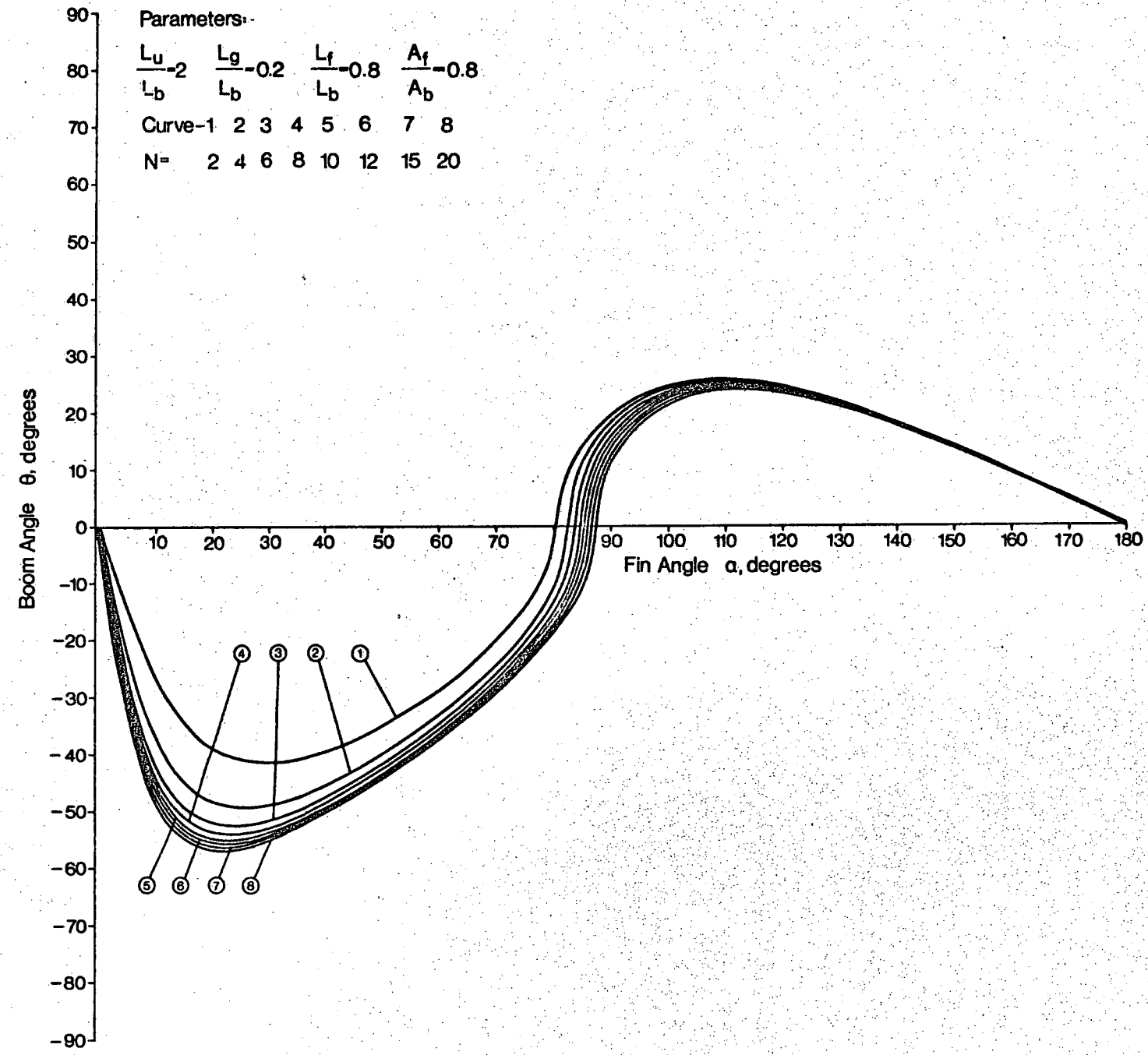

Fig.4 Boom Angle and Fin Angle relationship for different numbers of units.

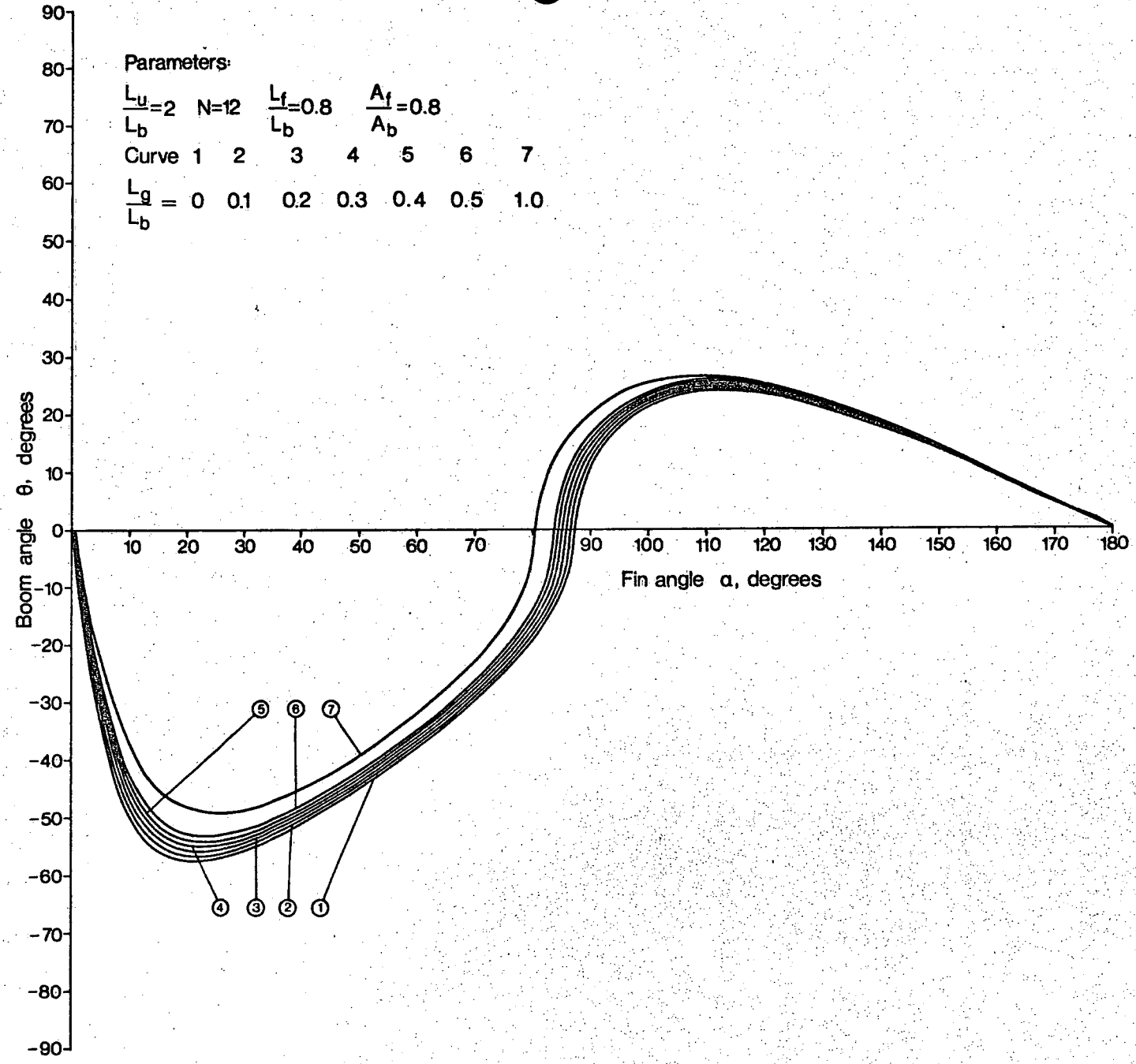

Fig.5 Boom Angle relationship for different fin gap widths

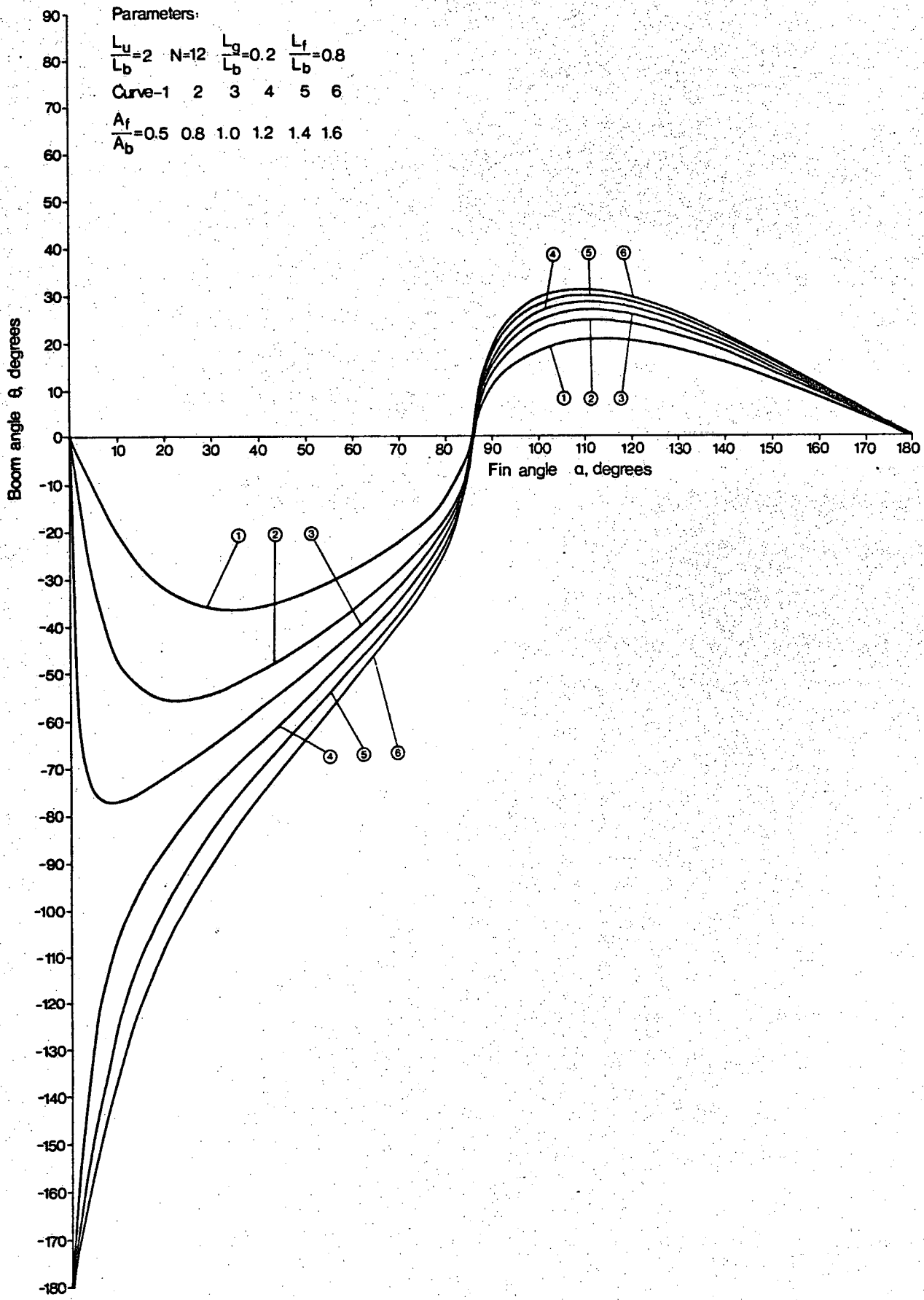

Fig.6 Boom Angle and Fin Angle relationship for different Fin Areas.

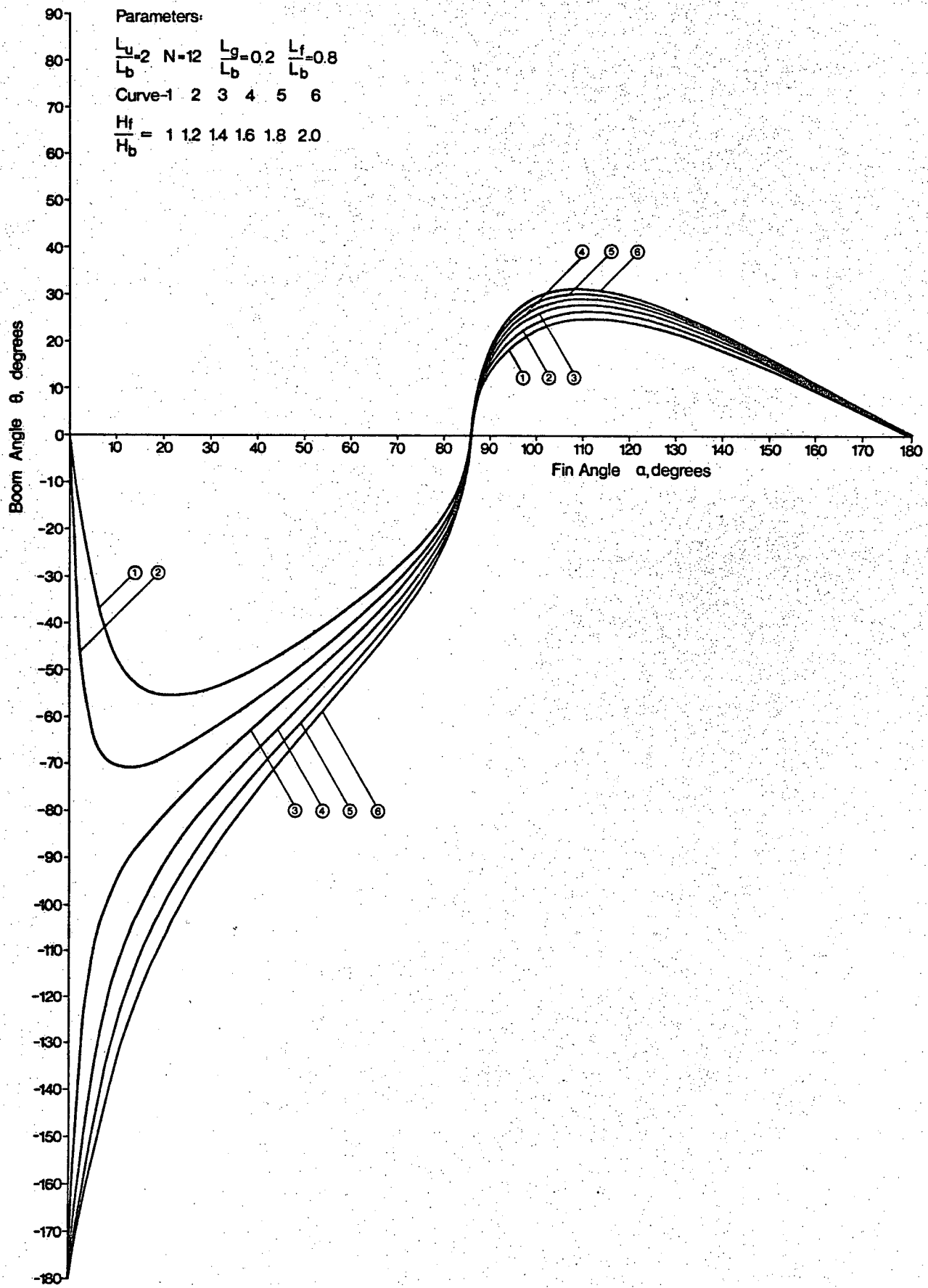

Fig. 7 Boom Angle and Fin Angle relationship at different Fin depths

Eventually, when the fins are completely closed, the boom will, theoretically point upstream. Such a boom position, of course, would never occur in reality because it is at unstable equilibrium like a needle standing on its tip. The slightest disturbance in the flow will upset the equilibrium and cause the boom to swing downstream. A right-swinging boom, or the lower half of the curves, of course, is of academic interest only as far as the development of the ice-oil boom is concerned.

Figure 8 shows θ-α curves of different L_f/L_b ratios. For the plottings the depth ratio of the fin is kept constant of $H_f/H_b=1$. It is seen from Figure 8 that the curves are of similar shapes to those of Figures 6 and 7. This should be expected because they all reflect the effect of increasing fin area on the boom angle. It is seen from comparing the upper part of the curves on Figures 7 and 8 that the increasing of fin area by increasing the fin length is more effective to increase the boom angle than increasing the depth of the fin. For instance, the comparison of curves 2 and 5 in Figure 8 shows that, when the area of the fin is doubled by increasing L_f/L_b from 0.8 to 1.6, the maximum boom angle θ_{max} is increased by a little more than 8^o. This is more than an increase of a little less than 7^o when the fin area is doubled by doubling the boom's depth as shown in Figure 7.

From Figures 3 to 8 and the discussions about them, one sees that the ice-oil boom should be initially deployed with its fins completely open. Then, it can be brought into the current by gradually closing the fin until the maximum boom angle is reached. The nearly linear curve of the θ-α curves at high fin angles means the swinging of the boom into the current is almost proportional to the change of the fin angle. Such a characteristic, of course, would make the operation of the boom much easier. From the curves, one also sees that they are quite flat near the θ_{max} point. This means that θ_{max} is insensitive to the fin angle around the optimal fin angle α_{max}. For field operation of a boom where strict operational control is difficult, such a relaxed operational requirement is very desirable.

For better visualizing the parametric effect on the maximum boom angle θ_{max} and the corresponding optimal fin angle α_{max}, θ_{max} and α_{max} are plotted against the different parameters L_u/L_b, N, L_g/L_b, A_f/A_b, H_f/H_b and L_f/L_b as shown in Figure 9. From Figure 9, one again sees the insensitivity of θ_{max} to the change in L_u/L_b, N and L_g/L_b. Although θ_{max} increases with the increase of the

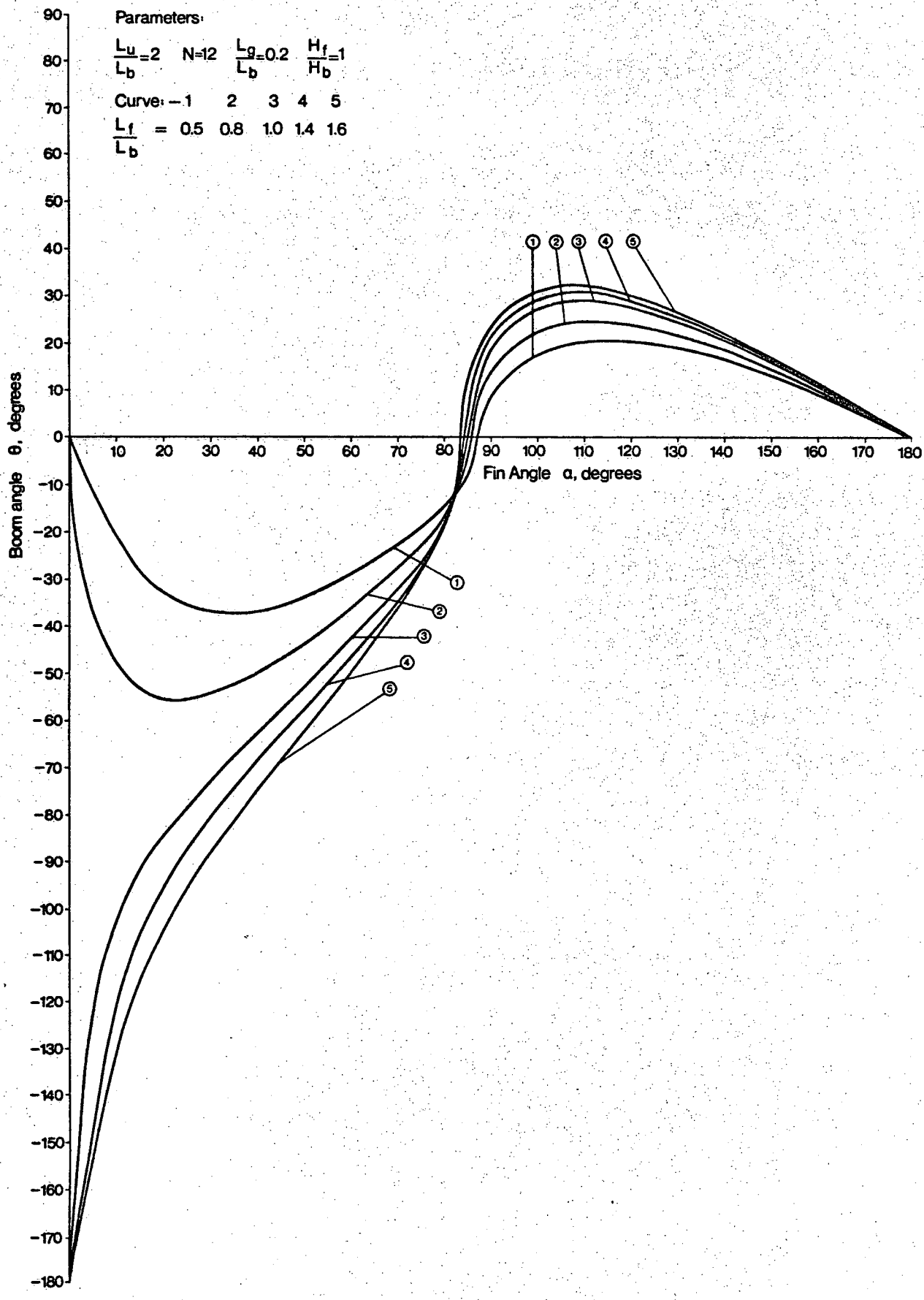

Fig.8 Boom Angle and Fin Angle relationship at different fin lengths

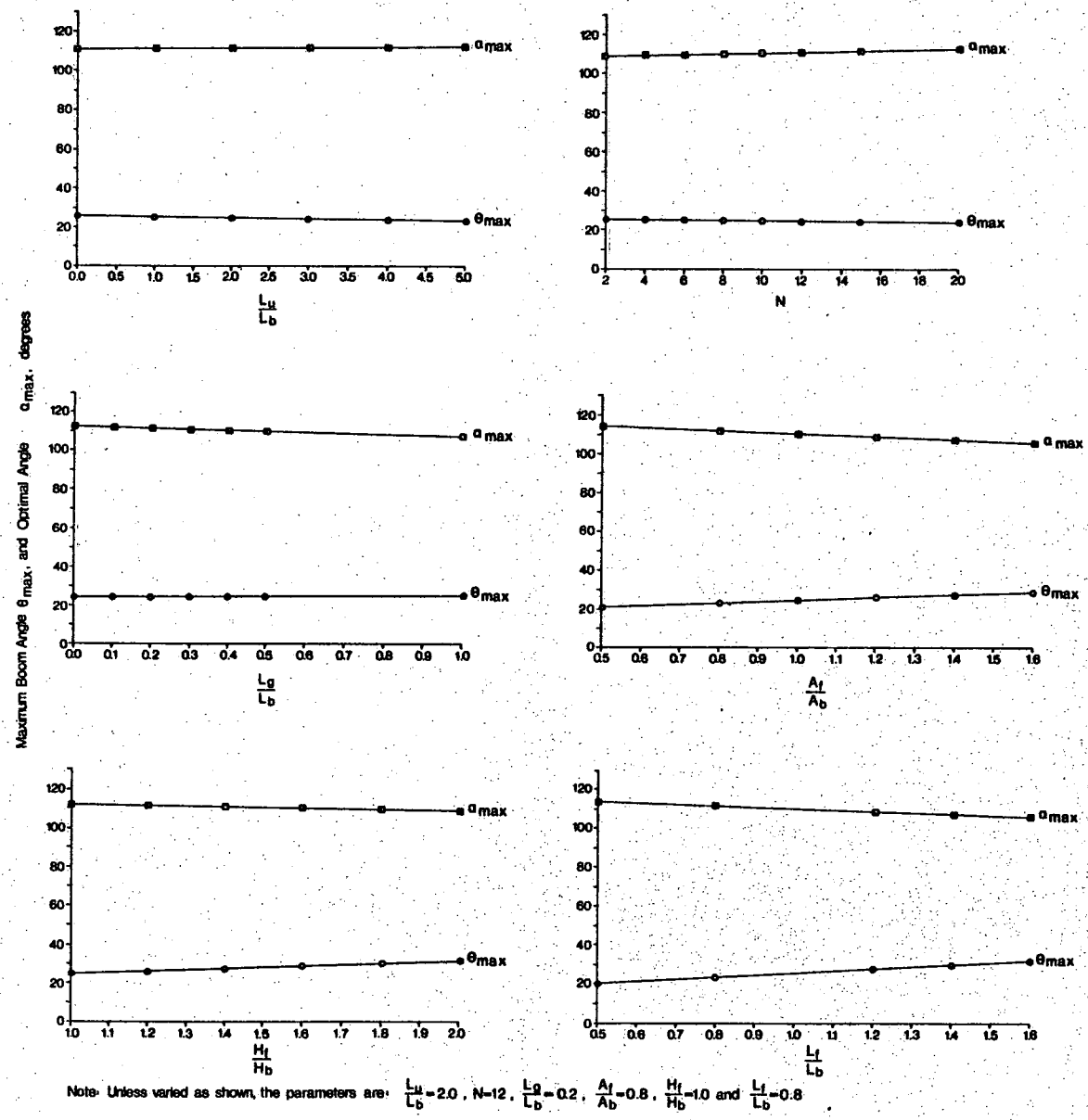

Fig. 9 Maximum Boom Angle and the Corresponding Optimal Fin Angle under Different Parametric Conditions

fin area, either by increasing the fin depth or the fin length, the increase is moderate and almost linear. From the diagrams, it is seen that with engineeringly practical dimensions, an ice-oil boom probably should be expected to make an angle of about 30° with the current and the optimal fin angle would be about 110°.

2.5 Restoring Moment of an Offset Boom

From the last section, one sees that under a given set of parametric conditions, there always exists an optimal fin angle α_{max} at which the boom will make the maximum angle θ_{max} with the current. Under working conditions, a boom should be so deployed that the fin angle is α_{max} and the boom angle is θ_{max}.

If, for one reason or the other, the boom angle of a working boom is changed to θ, an unbalanced, restoring moment will be resulted. The restoring moment tends to bring the boom back to its original position until $\theta=\theta_{max}$ again. The restoring moment is produced by the changes of the moments acting on the boom and on the fins.

The moment acting on the boom is given by Equation 8. the substitution of θ_{max} into the equation gives the moment on the boom at the equilibrium position $M_{b\ max_*}$ and the substitution of θ into the equation gives the moment on the boom at the new boom position M_{b_*}. From M_{b_*} and $M_{b\ max_*}$ one obtains the change of the moment acting on the boom

$$\Delta M_{b_*} = M_{b_*} - M_{b\ max_*} = A\,(\sin^2\theta - \mathrm{Sin}^2\,\theta_{max}) \qquad (19)$$

where

$$A = \frac{L_u}{L_b}\left(\frac{1}{2}\frac{L_u}{L_b} + N\right) + \frac{N^2}{2} \qquad (20)$$

In writing Equation 19, only the practically important case that the boom is deflected by the current to the left is considered. One also assumes $A_u/A_b=L_u/L_b$. By writing $\theta=\theta_{max}-\Delta\theta$, Equation 19 can be rewritten as

$$\Delta M_{b_*} = \frac{A\ \mathrm{Cos}\ 2\theta_{max}}{2}\ (1 - \mathrm{Cos}\ 2\Delta\theta - \tan 2\,\theta_{max}\ \mathrm{Sin}\ 2\Delta\theta) \qquad (21)$$

which is the reduction of the moment on the boom body itself due to the reduction of the boom angle $\Delta\theta$.

The moment acting on the fins in normalized form is given by Equation 9. The substitution of $\theta=\theta_{max}$ and $\alpha=\alpha_{max}$ into the equation gives the moment on the fins at the original boom position $M_{f\,max_*}$ and the substitution of $\theta=\theta$ and $\alpha=\alpha_{max}$ into the equation gives the fin moment at the new boom position M_{f_*}. From these two moments, it can be shown that the change in the moment on the fins (M_{f_*} - $M_{f\,max_*}$) is given by

$$\Delta M_{f_*} = \frac{(C \cos \alpha_{max} - B) \cos (2\alpha_{max} + 2\theta_{max})}{2} \left[1 - \cos 2\Delta\theta - \tan(2\alpha_{max} + 2\theta_{max}) \sin 2\Delta\theta\right] \tag{22}$$

where

$$B = \frac{A_f}{A_b} N \left(\frac{L_g}{L_b} + \frac{L_f}{L_b} \right) \tag{23}$$

and

$$C = \frac{A_f}{A_b} N \left(\frac{L_u}{L_b} + \frac{N+1}{2} \right) \tag{24}$$

The algebraic sum of Equations 21 and 22 gives the restoring moment of the offset boom

$$\Delta M_* = \Delta M_{b_*} + \Delta M_{f_*} \tag{25}$$

In the last section, the values of α_{max} and θ_{max} for different sets of parameters have been calculated. Based on these α_{max} and θ_{max} values and Equations 21, 22 and 25, curves of ΔM_{b_*}, ΔM_{f_*} and ΔM_* versus $\Delta\theta$ curves can be calculated and plotted for different parametric conditions as shown in Figures 10 to 14.

Figure 10 shows the restoring moment versus the offset angle curves, or specifically, the ΔM_{b_*}, ΔM_{f_*} and ΔM_* versus $\Delta\theta$ curves, at different L_u/L_b ratios. It is seen from the curves that the upstream protective length of the boom L_u has a noticeable effect on the restoring moments of the boom. It is interesting to note from Figure 10 that under the selected parametric conditions, the total restoring moment of the boom, i.e. ΔM_*, is caused more by the reduction of the counterclockwise moment on the boom body than by the increase in the clockwise moment on the fins. It is also interesting to see from Figure 10 that while the ΔM_{b_*} versus $\Delta\theta$ curves become flatter at higher $\Delta\theta$ values, the ΔM_{f_*} versus $\Delta\theta$ curves are more or less linear for the whole $\Delta\theta$ range. By comparing the ΔM_*-$\Delta\theta$ curves, one sees that the effect of L_u/L_b on ΔM_* is almost proportional to the value of L_u/L_b.

It should be noted that as far as the design and performance of an ice-boom are concerned, one is only interested in the ΔM_*-$\Delta\theta$ curves. The several selected ΔM_{b_*}-$\Delta\theta$ and ΔM_f*-$\Delta\theta$ curves are for the purpose of assisting one to see the physical insight. It should also be noted that according to Equations 21, 22 and 25, the restoring moments ΔM_{b_*}, ΔM_{f_*} and ΔM_* calculated are all negative values, indicating that they are clockwise moments. For better graphical presentation, however, they are shown as positive quantities in Figure 10.

Figure 11 shows restoring moment curves of different N values. One sees from these curves the great effect of the number of boom units on the restoring moment ΔM_*. The effect of N on ΔM_* is more prominent at higher N numbers. This means that it is more effective to add five units to a 15-unit boom, say, than to a 10-unit boom for increasing the restoring moment. The ΔM_{b_*}-$\Delta\theta$ and ΔM_{f_*}-$\Delta\theta$ curves in Figure 11 again are for supplementary purposes only. These curves show similar characteristics as those shown in Figure 10.

In Figure 12 are the restoring moment curves for booms of different L_g/L_b ratios. From the curves one immediately sees that the effect of L_g/L_b on ΔM_*, ΔM_{b_*} and ΔM_{f_*} is limited. Therefore, to increase the gap width of the fins is not a practical way for increasing the restoring moments.

Figure 13 shows restoring moment curves of different L_f/L_b values. It is seen from these curves that the fin length L_f influences ΔM_* greatly. For increasing the restoring moment of a boom, it is practical to increase the fin length. From the supplementary ΔM_{b_*} and ΔM_{f_*} curves, one sees that the fin length has a greater effect on ΔM_{f_*} than on ΔM_{b_*}. While for booms of low L_f/L_b

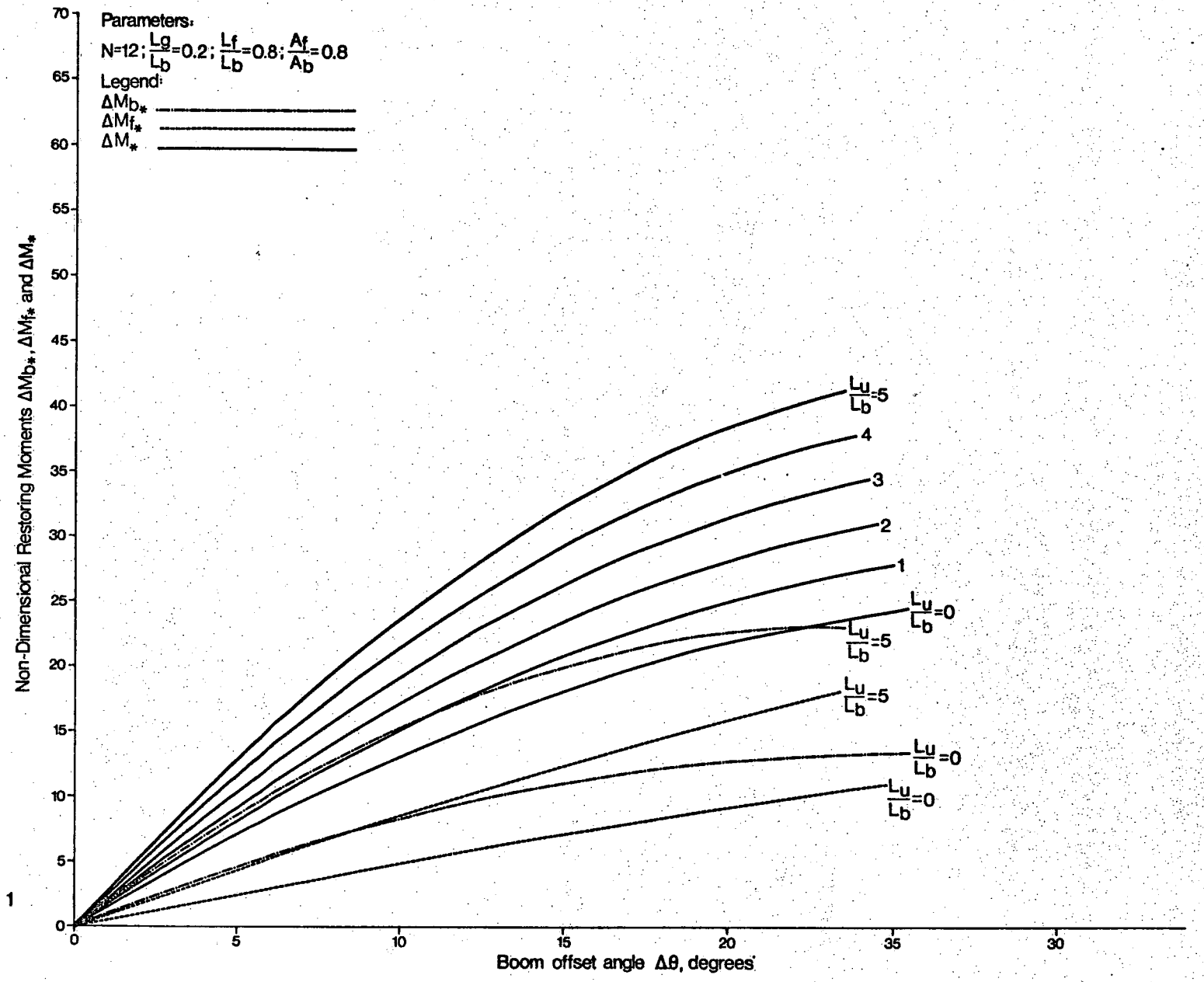

Fig 10 Relationship between Restoring Moment and Offset angle for Booms of different upstream protective lengths

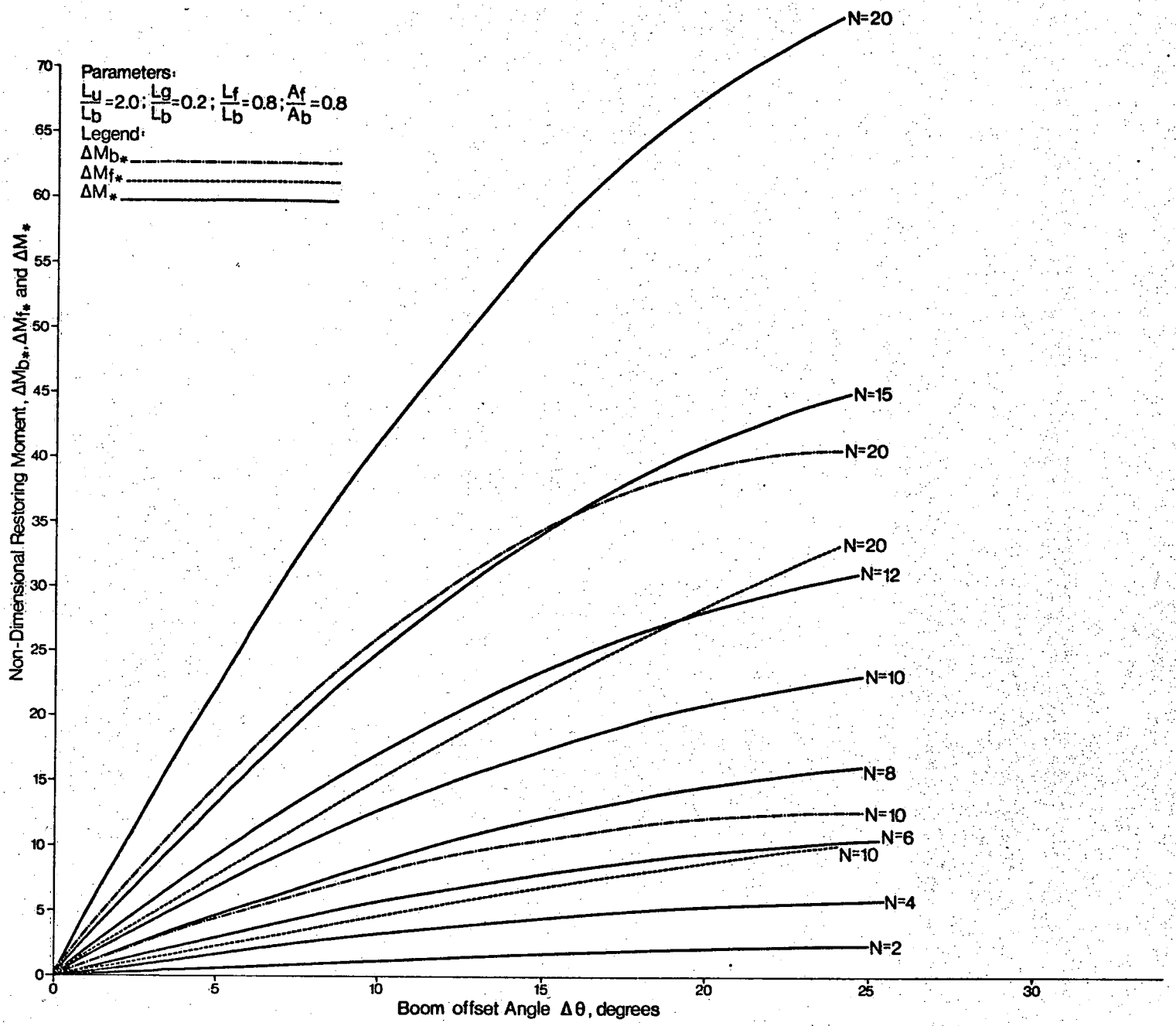

Fig 11 Relationship between Restoring Moment and Offset angle for booms of different Number of units

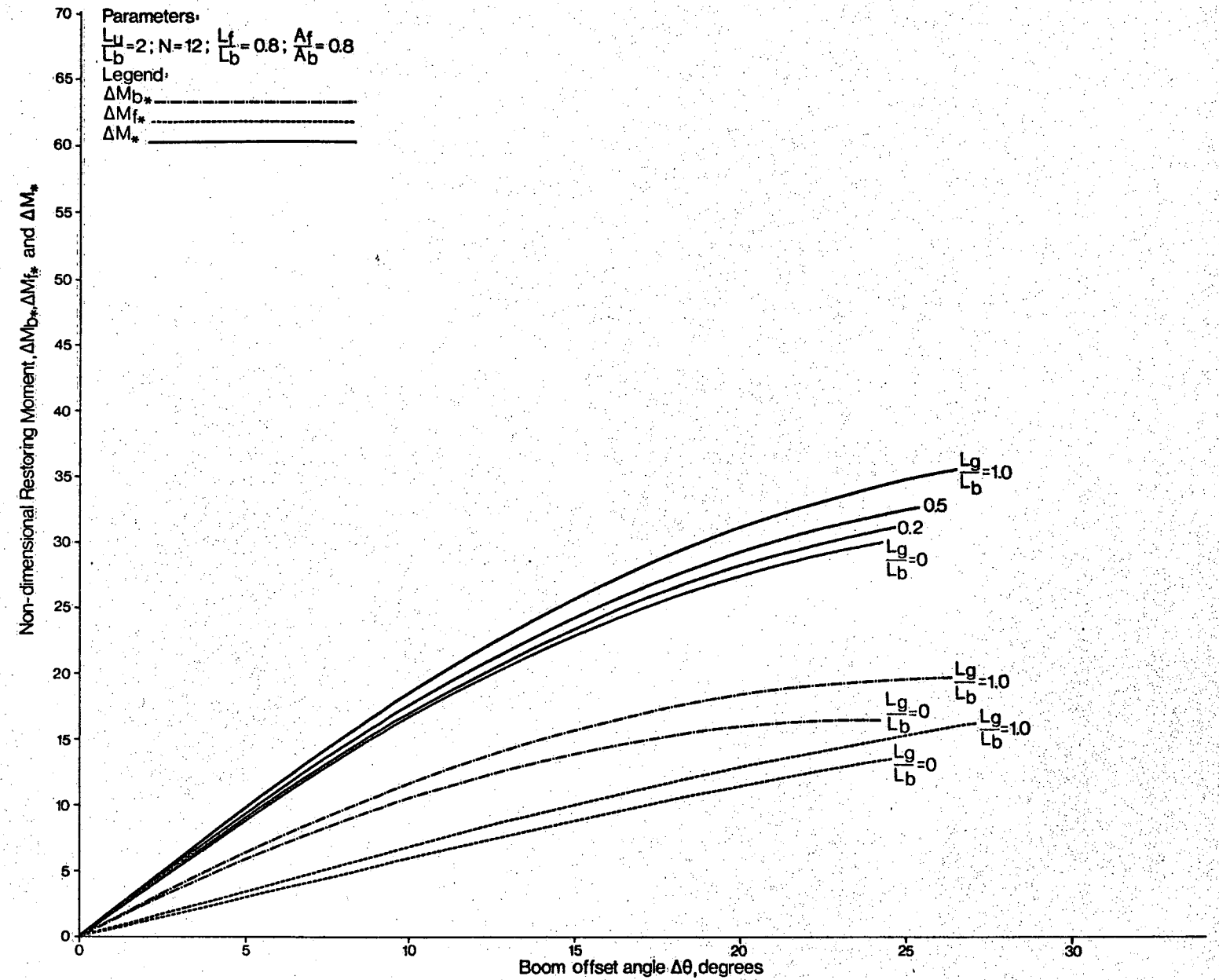

Fig 12 Relationship between Restoring Moment and Offset Angle for Booms of different fin gap widths

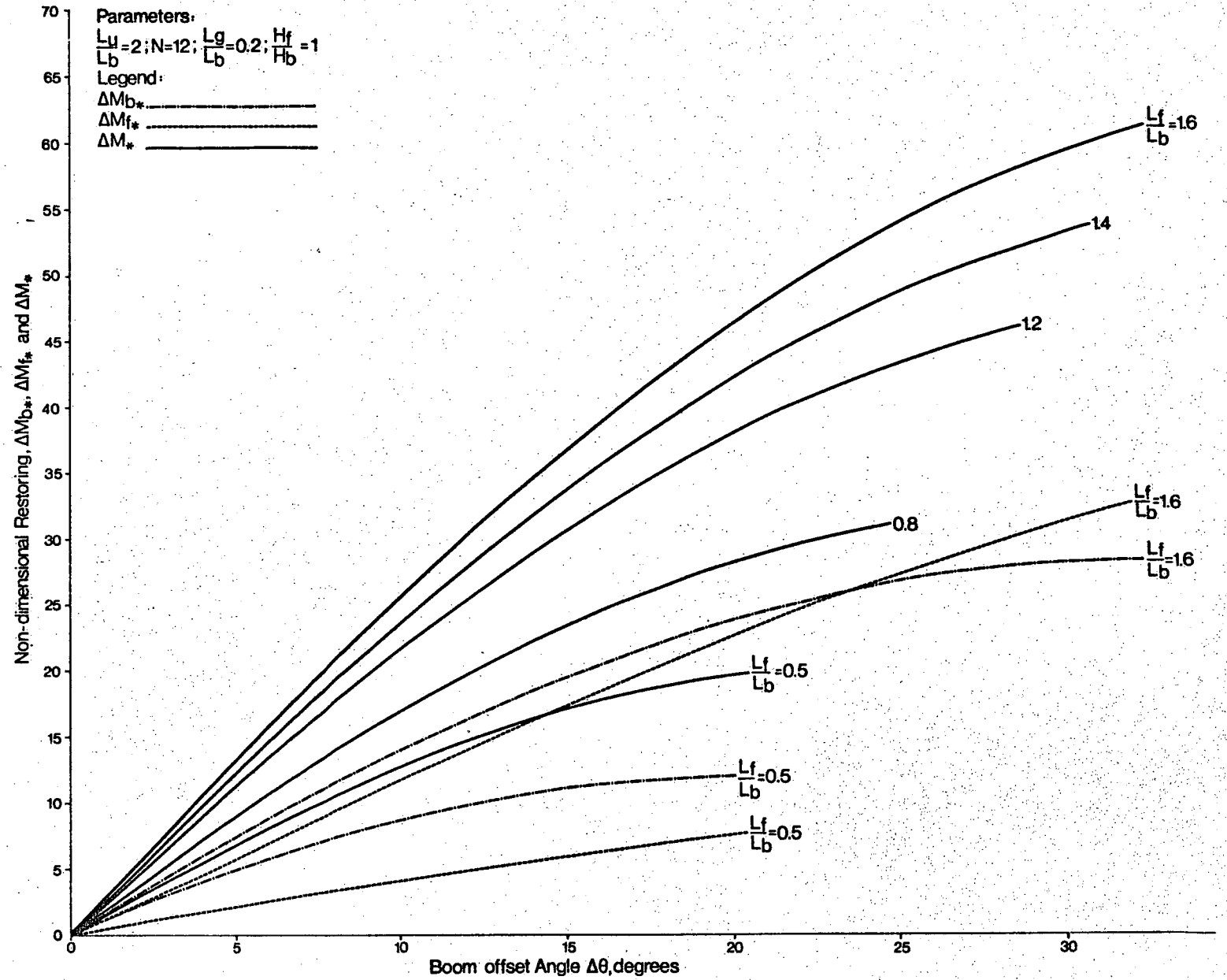

Fig13 Relationship between Restoring Moment and Offset angle for booms of different fin lengths.

ratios, the restoring moment of the boom ΔM_* is largely contributed by ΔM_{b_*}, for booms of large L_f/L_b ratios, ΔM_{f_*} becomes the major contributor.

In Figure 14 are restoring moment curves under different A_f/A_b ratios. While the fin area is varied, the fin length is maintained the same. This means that the fin area is changed by varying the fin's depth. It is seen from the curves that the fin area ratio A_f/A_b (or the depth ratio) also has a great effect on the restoring moment of the boom. The overlaying of Figure 14 over Figure 13, however, reveals that it is slightly more advantageous to increase ΔM_* by increasing L_f than by increasing H_f for the same fin area. From the supplementary ΔM_{b_*} and ΔM_{f_*} curves, one also again sees the greater effect of A_f/A_b on ΔM_{f_*} than on ΔM_{b_*}.

For effectively deflecting ice floes, a boom should produce a large restoring moment when it is offset. From the above discussions, one sees that the best way is to use as many units as possible in the boom and for each unit, the fin should be made as long as engineeringly and operationally permissible.

2.6 Stopping of Ice Floe by Boom

Figure 15 shows the stopping of an ice floe by a boom. Before the arrival of the ice floe, the boom is at an angle of θ_{max} to the flow. As the ice floe hits the boom, the boom yields and a restoring moment as discussed in the last section is produced. The yielding continues until the normal kinetic energy of the ice floe to the boom is exhausted and the boom angle reaches its minimum value of θ_{mini}. Thereafter, the boom begins to swing back to its original position under the restoring moment and in the process imparts normal momentum in the opposite direction back to the ice floe should it not have left the boom.

In this section, the relationship between the size of the ice floe and the yielding angle ($\theta_{max} - \theta_{mini}$) will be studied. To simplify the mathematical modelling, it is assumed that:

1. After hitting the boom, the ice floe will not rotate, so no linear kinetic energy is transformed into rational kinetic energy.
2. The friction between the ice floe and the boom is negligible.
3. The loss of kinetic energy due to the initial impact between the ice floe and the boom is negligible, and
4. There is little displacement of the boom other than rotation.

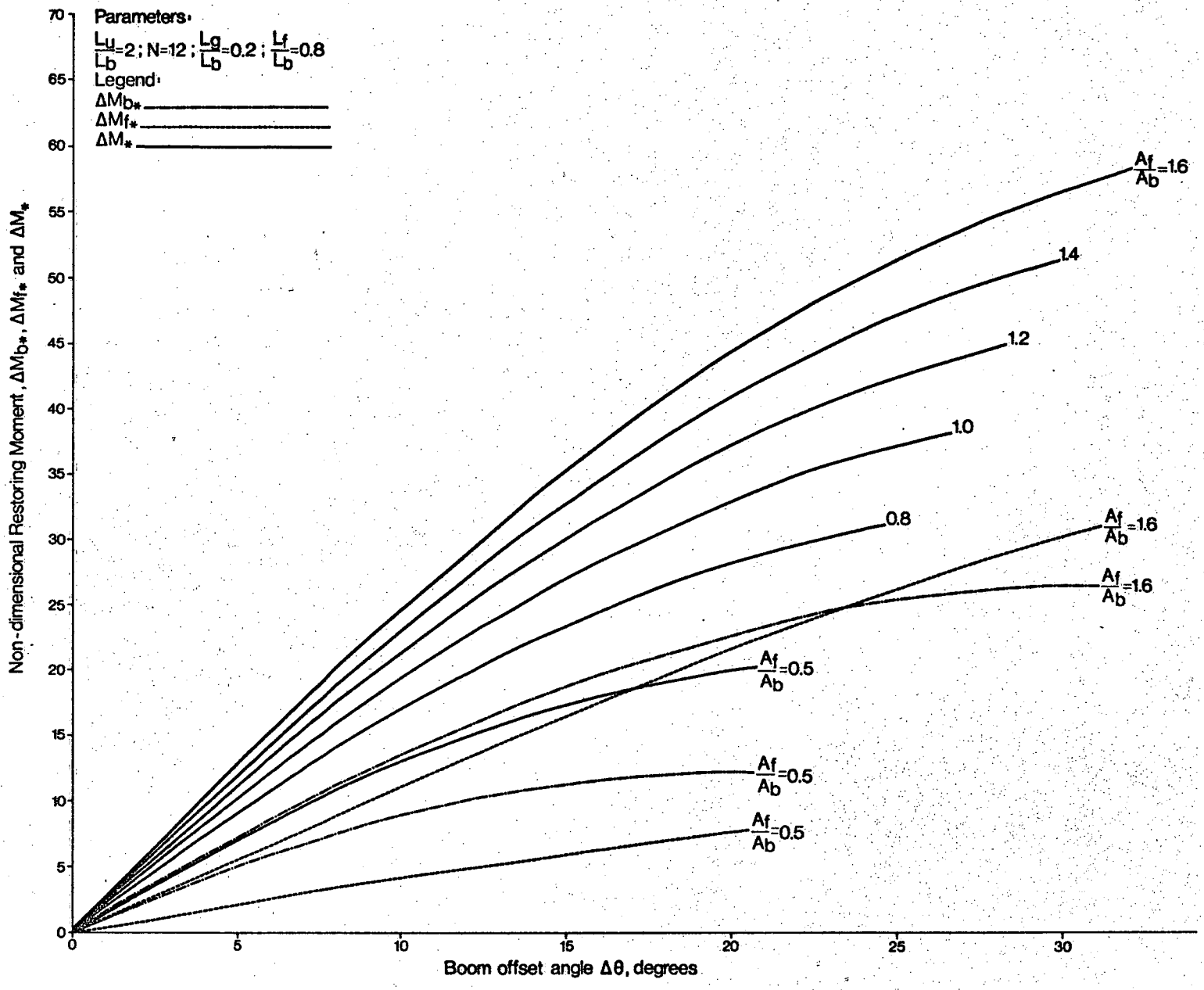

Fig 14 Relationship between Restoring Moment and Offset angle for booms off different fin areas.

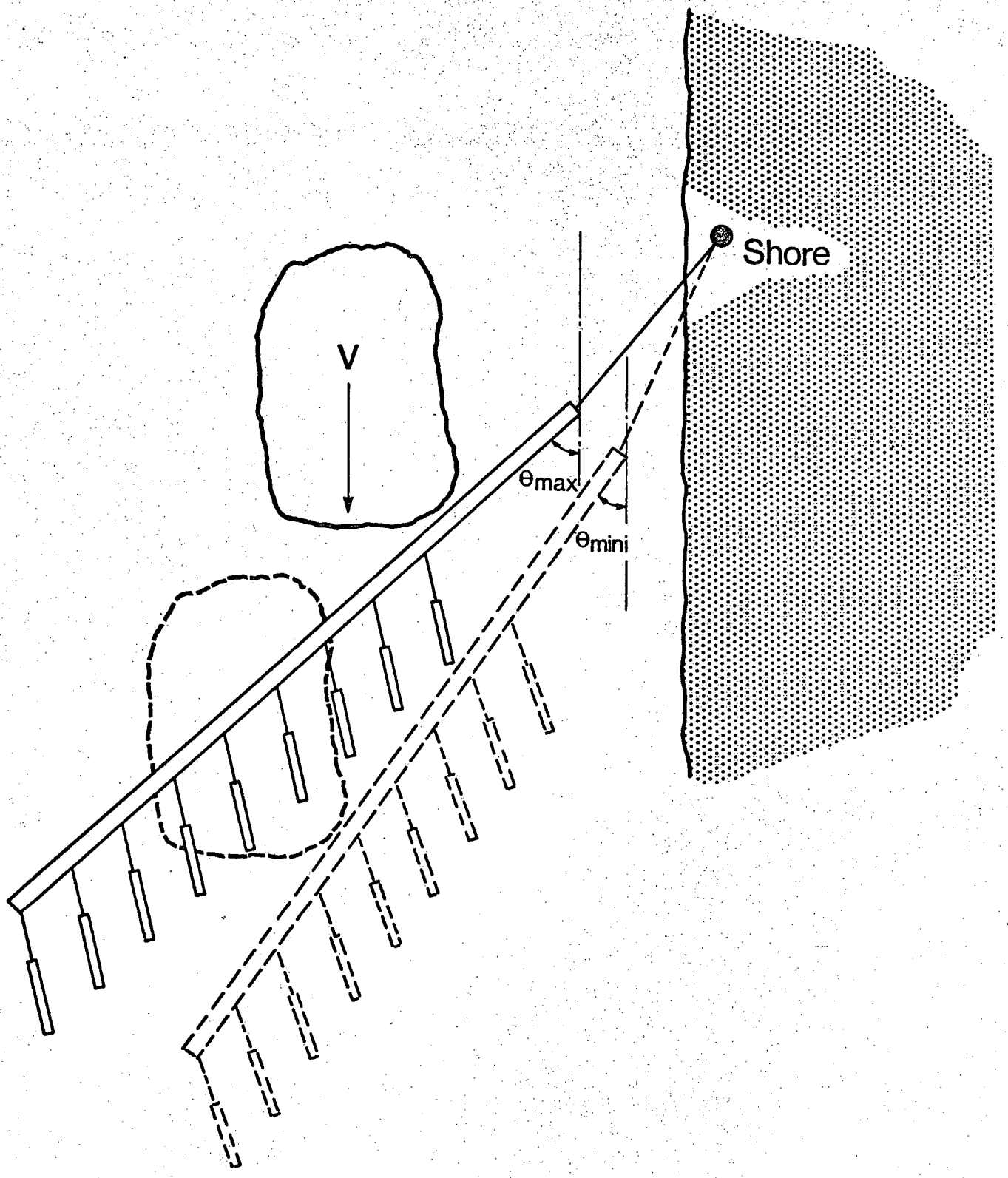

Fig15 Deflection of an ice floe by boom

At minimum boom angle θ_{mini}, the normal velocity of the ice floe to the boom is zero. The loss of kinetic energy of the ice floe in the direction normal to the boom, therefore, is

$$\Delta E_K = \frac{1}{2} (\rho_i A_i t_i) \eta V^2 \sin^2 \theta_{mini} \quad (26)$$

where ρ_i is the density of the ice floe, A_i is the area of the ice floe, t_i is the thickness of the ice and η is the coefficient of virtual mass. According to the theory of hydrodynamics (Lamb, 1932), the stopping of an object moving in air and in water, say, is different because in the latter case the water that moves with the object has to be put to rest also. The net effect of this is an equivalent increase of the mass of the object by a multiplying factor η greater than unity. For a cylinder made of a material of the density of water, for instance, the value of η is two if the cylinder is moving in water.

Because the normal Kinetic energy is used to overcome the restoring moment, one may write the following equation

$$\frac{1}{2}(\rho_i A_i t_i)\eta V^2 \sin^2 \theta_{mini} + \frac{1}{2} C_D \rho V^2 A_b L_b \int_{\theta_{max}}^{\theta_{mini}} \Delta M_* \, d(\Delta\theta) = 0 \quad (27)$$

In the above equation, the second term is the work done by the restoring moment and the integration is the area under ΔM_*-$\Delta\theta$ curve between θ_{max} and θ_{mini}. Writing $\Delta\theta=\theta_{max}-\theta_{mini}$, $K=\rho C_D/\rho_i \eta$ and noting that $A_b=H_b L_b$, from Equation 27 one obtains

$$V_{i_*} = \frac{1}{K} \frac{A_i t_i}{L_b^2 H_b} = \frac{\int_{\Delta\theta} \Delta M_* \, d(\Delta\theta)}{\sin^2 (\theta_{max} - \Delta\theta)} \quad (28)$$

If V_{i_*} is considered as the dimensionless volume of the ice floe, the above equation relates the size of the floe and the yielding angle of the boom. The constant K may be obtained experimentally.

In the last section it has been shown that for a given set of parameters, there exists an optimal fin angle α_{max} and a maximum boom angle θ_{max} and based on them a ΔM_* versus $\Delta\theta$ curve can be calculated and plotted. Using the θ_{max} value and the ΔM_*-$\Delta\theta$ curve so obtained, a curve of V_{i_*} versus $\Delta\Theta$ may be evaluated and plotted according to Equation 28. Following the above route, V_{i*}

versus $\Delta\Theta$ curves under different parametric conditions were plotted as shown in Figures 16 to 20.

In Figure 16 are V_{i_*} versus $\Delta\Theta$ curves of different parametric L_u/L_b values. From the curves one sees that a boom with a longer upstream protective section L_u will yield less when hit by an ice floe of certain size than a boom with a shorter L_u. However, since a boom with a shorter L_u attains a larger maximum boom angle (see Figure 3), the final angle between the boom and the flow will be about the same both for booms of large L_u values and booms of small L_u values. The conclusions drawn thus is that although the upstream, unfinned section of a boom may serve to protect the fins downstream from ice damages, it affects little the boom angle and the size of the ice floe that is deflected by the boom when the boom yields to a certain angle.

In Figure 17, V_{i_*} is plotted against $\Delta\Theta$ for different N values. From the curves one sees that the number of units of a boom has a great effect on the size of the ice floe that can be deflected by the boom for a given yield angle. The great effect of N on V_{i_*} can be easier appreciated if one notes that the latter is plotted on the logarithmic scale.

Figure 18 shows the V_{i_*} versus $\Delta\Theta$ curves of different parametric L_g/L_b ratios. Since the curves crowd together, it means that the gap width of the fin has little influence on the size of the ice floe that can be deflected by the boom for a given yield angle. In fact, the lower positioning of the V_{i_*} -$\Delta\Theta$ curves of higher L_g/L_b values means that a boom with a bigger fin gap will even yield more when hit by an ice floe of a given size. Since a wider fin gap increases slightly the maximum angle of the boom with the current (see Figure 5), the final angle of the boom with the current therefore would be about the same when hit by an ice floe of given size, regardless of the value of L_g. In conclusion, one may say that the fin gap with L_g is not a critical design criterion.

In Figure 19 are V_{i_*} versus $\Delta\Theta$ curves of different A_f/A_b ratios. It is seen from the curves that the area of the fins affects the V_{i_*} versus $\Delta\Theta$ curves greatly, not that much on the angle of yield when the boom is hit by a floe of given size; in fact the yield angle is even larger for booms of larger fin areas, but on the maximum boom angle which leads to a greater boom angle to shield the area behind the boom.

In Figure 20 are V_{i_*} versus $\Delta\Theta$ curves of different L_f/L_b ratio. One sees that these curves are similar to the curves in Figure 19. This, in fact, should be

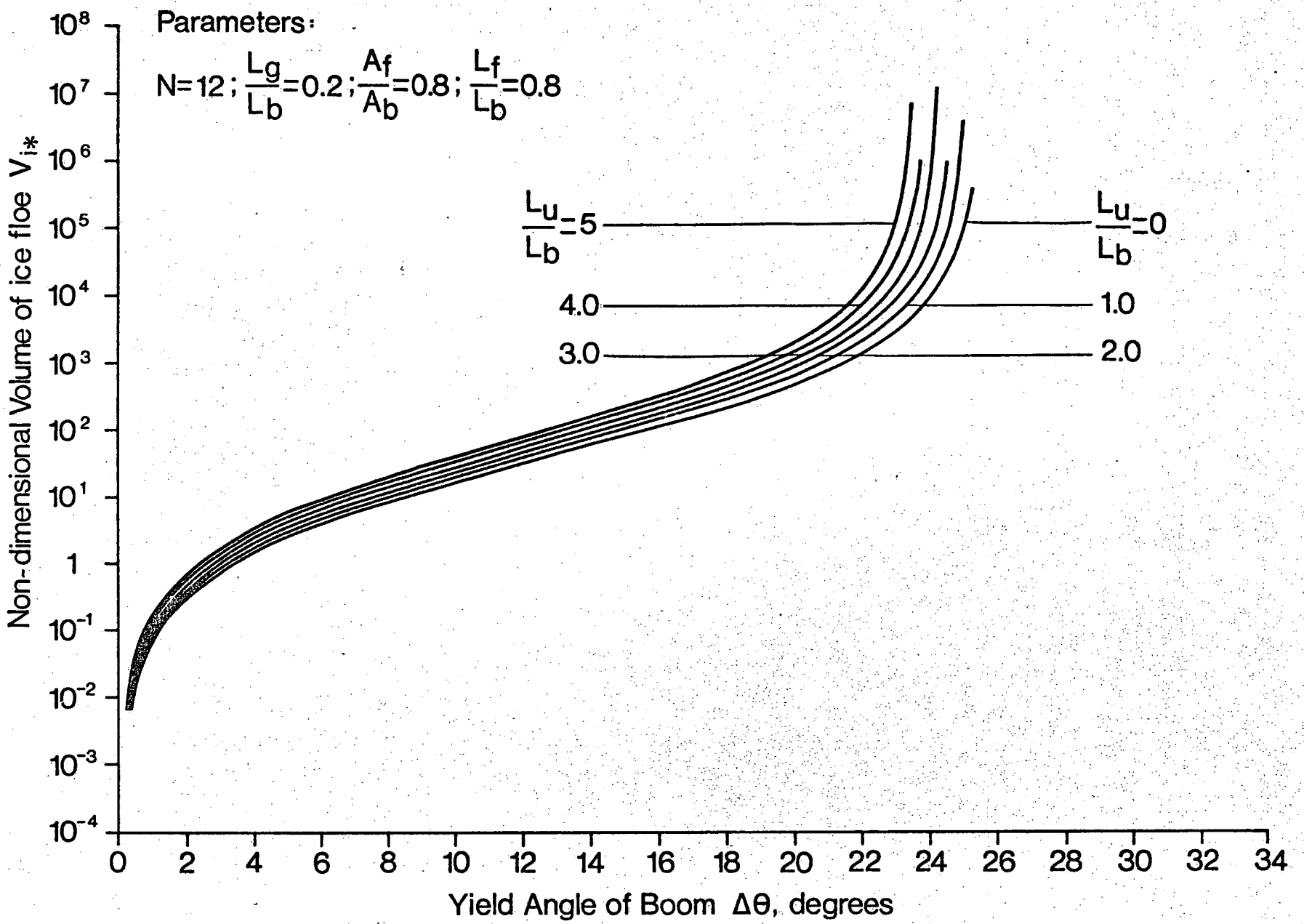

Fig 16 Relationship between size of ice floe and yield angle for booms of different upstream protective lengths

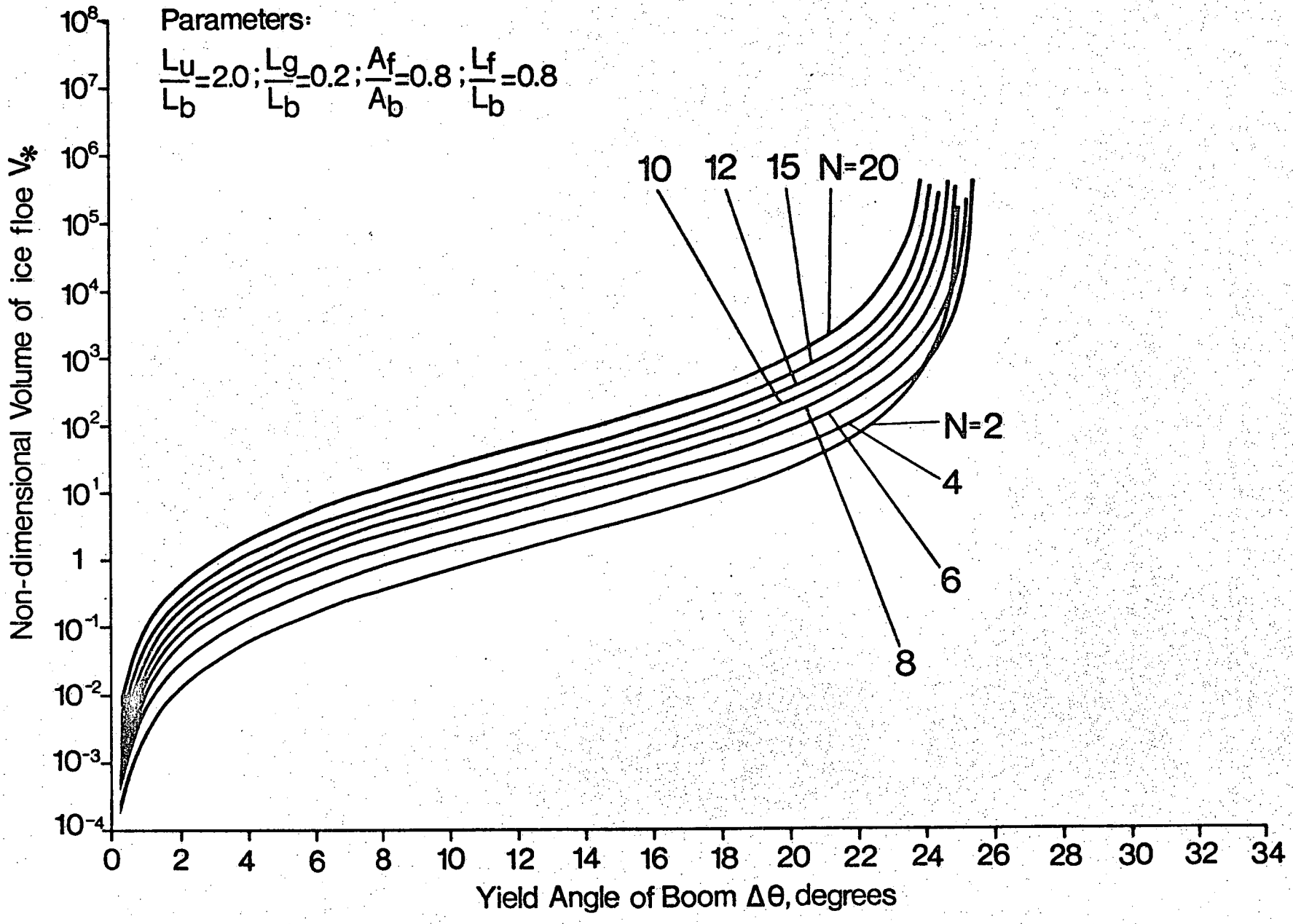

Fig17 Relationship between size of ice floe and and Yield Angle for booms of different units

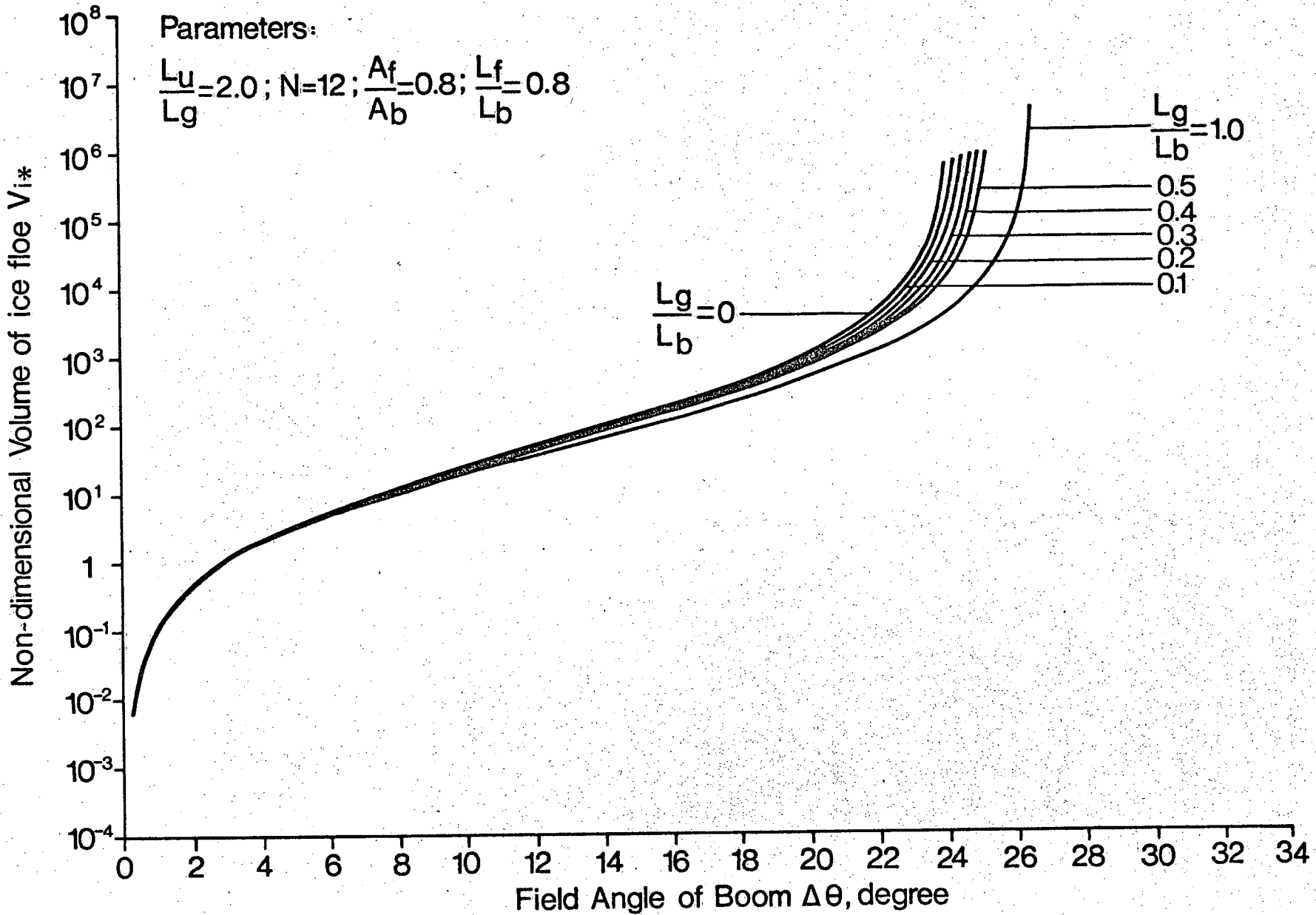

Fig 18 Relationship between size of ice floe and yield angle for booms of different fin gap widths

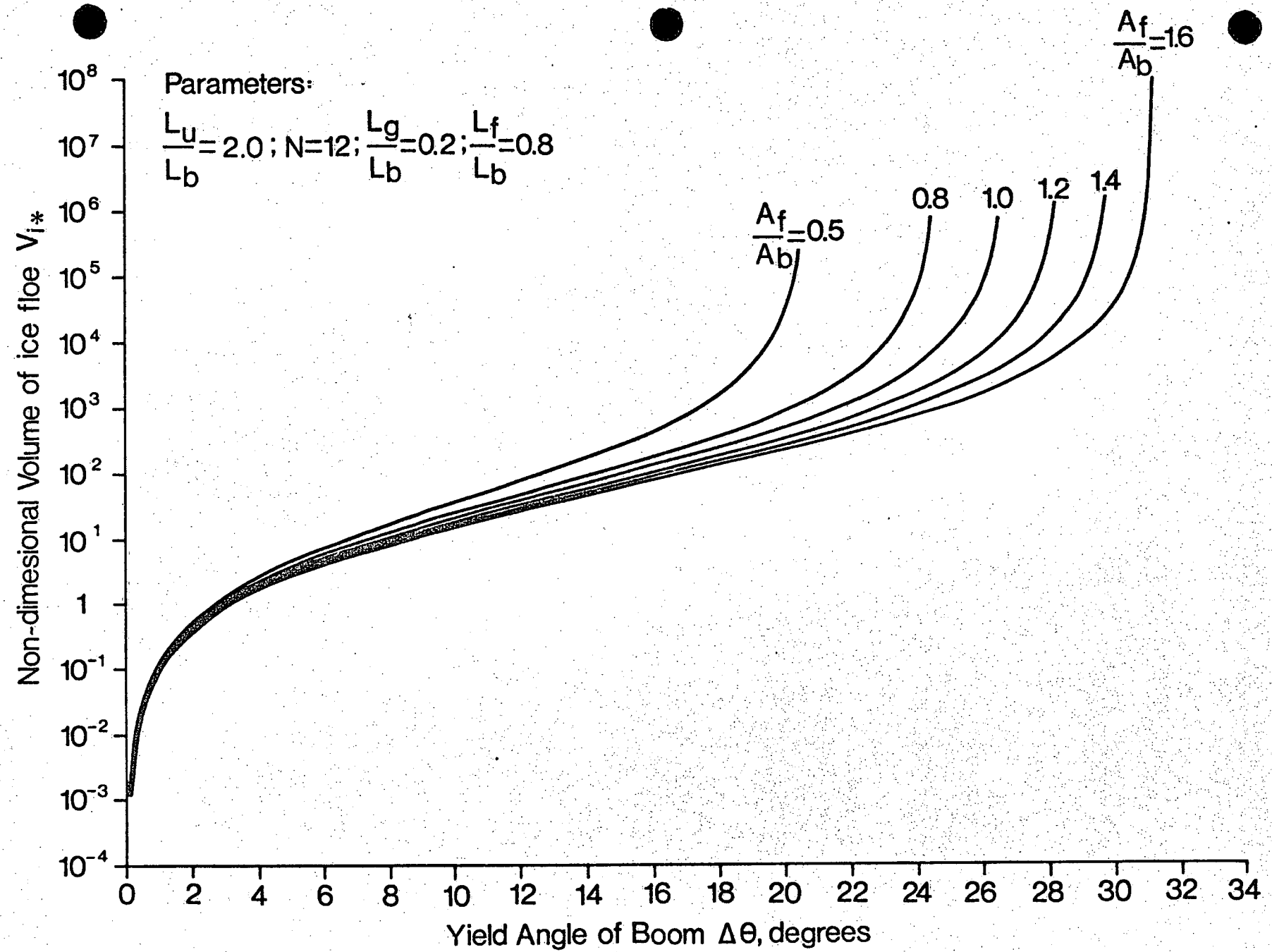

Fig 19 Relationship between size of ice floe and yield angle for booms of different fin areas

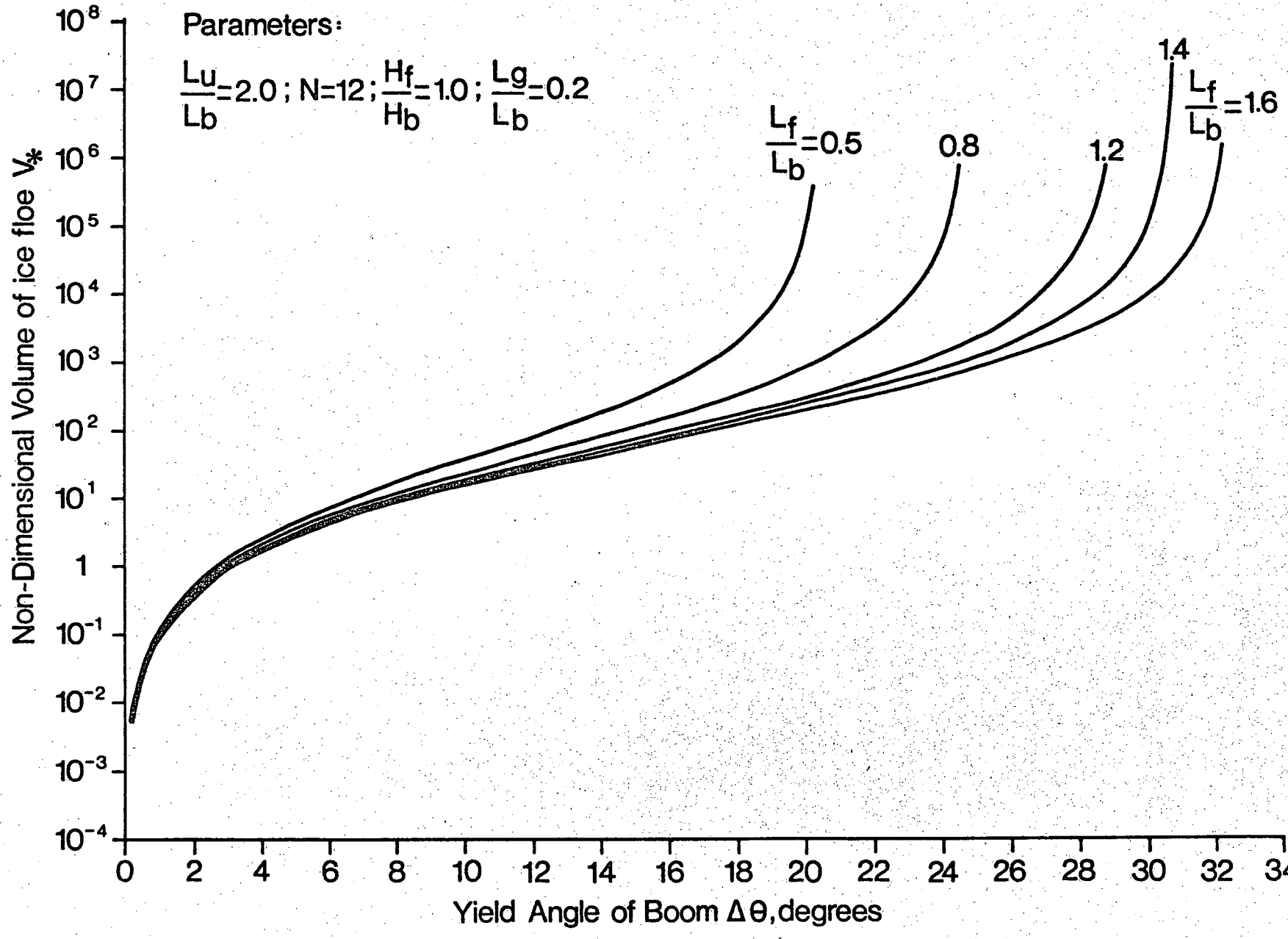

Fig 20 Relationship between size of ice floe and yield angle for booms of different fin lengths

expected because the curves in Figure 20 are plotted for $H_f/H_b=1$ so L_f/L_b really is a measure of A_f/A_b. The overlaying of Figure 19 and 20, however, reveals that for curves of A_f/A_b less than unity, the curves in Figure 19 are to the right of the corresponding curves in Figure 20 and for curves of A_f/A_b greater than unity, it is the other way around. This means that for a given fin area, it is better to increase the depth of the fin when $A_f/A_b<1$ and to increase the length of the fin when $A_f/A_b>1$.

It should be pointed out that the conclusions reached above not only are valid for a single ice floe, but for a group of ice floes also provided that the boom does not reach the minimum angle θ_{mini} when the last floe of the group hits it. In other words, when dealing with a group of ice floes, V_{i_*} should be considered as the combined nondimensional volume of the ice floes.

2.7 Drag on the Boom

Drag is produced by the current on the boom. For the design of shore anchors and the selection of anchoring cables, one needs to know the drag on the boom, both the magnitude and the direction.

Drags are produced on the boom body itself and on the fins. Following the convention adopted earlier, only the normal components of these drags are considered.

The normal drag, or the drag produced by the normal component of the velocity, on the boom body itself is given by (see Figure 2).

$$D_b = \frac{N}{2} C_D \rho V^2 \sin^2\theta H_b L_b + \frac{1}{2} C_D \rho V^2 \sin^2\theta H_b L_u \qquad (29)$$

where the first term on the right is the normal drag on the finned part of the boom of N units and the second term is the normal drag on the upstream protective section. By normalizing the drag force according to

$$D_{b_*} = \frac{D_b}{\left[\frac{1}{2} C_D \rho V^2 H_b L_b\right]} \qquad (30)$$

Equation 29 may be rewritten as

$$D_{b_*} = \sin^2\theta \left(N + \frac{L_u}{L_b}\right) \qquad (31)$$

The total normal drag on the N fins can be shown to be (refer to Figure 2)

$$D_f = \frac{N}{2} C_D \rho V^2 \sin^2(\alpha + \theta) H_f L_f \tag{32}$$

By normalizing D_f on the same basis as D_b, one obtains

$$D_{f_*} = \frac{N H_f L_f}{H_b L_b} \sin^2(\alpha + \theta) \tag{33}$$

For the coordinate system shown in Figure 2, the x components of D_{b_*} and D_{f_*} can be shown to be respectively

$$-D_{b_*} \cos\theta \quad \text{and} \quad -D_{f_*} \cos(\alpha + \theta)$$

and the y components to be respectively

$$D_{b_*} \sin\theta \quad \text{and} \quad D_{f_*} \sin(\alpha + \theta)$$

With the above force components, the total drag on the boom is seen to be

$$D_* = \left\{ \left[D_{b_*} \cos\theta + D_{f_*} \cos(\alpha+\theta) \right]^2 + \left[D_{b_*} \sin\theta + D_{f_*} \sin(\alpha + \theta) \right]^2 \right\}^{\frac{1}{2}} \tag{34}$$

and the angle between the resultant drag and the direction of flow is given by

$$\phi = \tan^{-1} \left[\frac{-D_{b_*} \cos\theta - D_{f_*} \cos(\alpha + \theta)}{D_{b_*} \sin\theta + D_{f_*} \sin(\alpha + \theta)} \right] \tag{35}$$

For practical purposes, only the case when the boom is deflected by the current to the left will be discussed here. From Equations 31, 33, 34 and 35, one sees that D_* and ϕ are functions of N, L_u/L_b, H_f/H_b, L_f/L_b, θ and α. Since it has been shown earlier in Section 2.4, θ is a function of the five other variables shown above plus the variable L_g/L_b, the plotting of D_* and ϕ under different parametric conditions therefore is possible. Because it has been shown that the effect of L_g/L_b on the θ-α relationship is small, a typical value of L_g/L_b b=0.2, say, may be used for the calculation of D_* and θ without loss of generality. From Equation 33, it is seen that the influence of H_f/H_b and L_f/L_b on D_{f_*} and,

consequently, on D_* and ϕ, is in the form of $H_f L_f/H_b L_b$. Therefore, one may vary the value of the above parameters by changing L_f/L_b only while maintaining H_f/H_b a constant, to be equal to unity, say.

According to the above discussion, D_* and ϕ are calculated and plotted under the following parametric conditions:

TABLE 2 PARAMETERS FOR CALCULATING TOTAL DRAG

N	2	4	6	8	10	12	15	20
L_u/L_b	2							
L_f/L_b	0.5	0.8	1.2	1.4	1.6			
L_g/L_b	= 0.2							
H_f/H_b	= 1.0							

In the above table, the underlined parametric values are for the reference case. In the comparative study, the underlined values are used except for the parameter which is being studied and which systematically changes its value according to the table. The D_* versus α and ϕ versus α curves are shown in Figure 21. In Figure 21, the points that corresponded to θ_{max} (or α_{max}) are noted for each curve.

Figure 21a and b are plottings for booms of different number of units N. It is seen from Figure 21a that the drag on the boom increases more or less proportionally with the number of boom units used in the boom. It is important to note that the drag on the boom progressively increases as the fins are gradually closed and the drag is not at its maximum when the boom makes the largest angle with the flow. From the plotting one sees that to avoid high stress on the boom and on the anchoring structure, a boom should always be deployed with the fins completely open and brought to the working position by gradually closing the fins.

According to the definition (see Figure 2), ϕ is the angle between the drag force and the shore. It is seen from Figure 21b that at large fin angles ϕ is negative, meaning the upstream end of the boom will be pressing against the shore. This, really, is desirable because it helps to seal the area behind the boom from ice entrance, although the boom may need to be pushed off from the shore

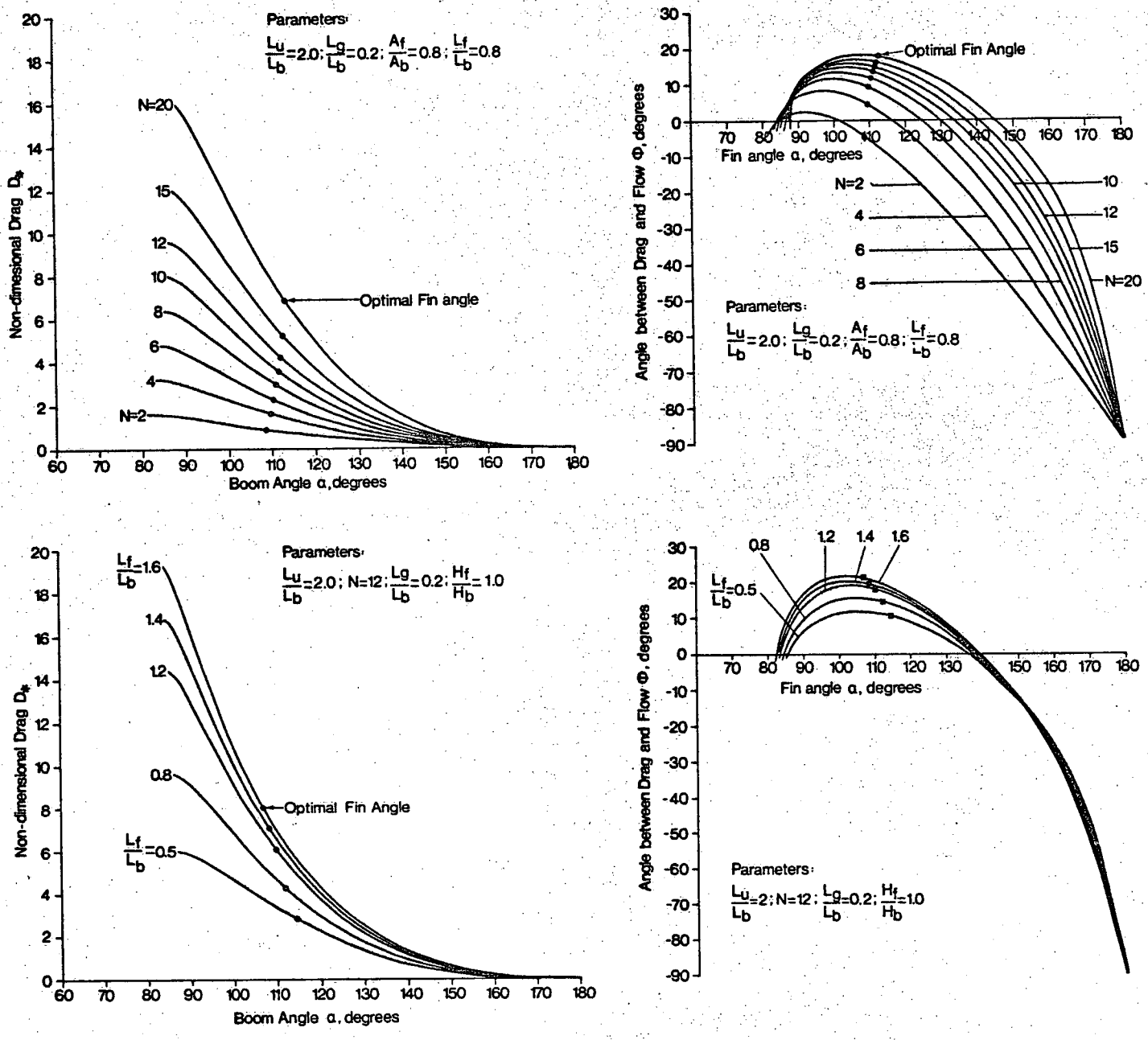

Fig 21 Drag on boom, magnitude and direction

for initial fin closing. Comparison of Figure 21b with Figure 4 shows that when a boom is at the optimal operational position, the angle between the drag and the shore ϕ is less than the maximum boom angle θ_{max}. The anchoring line, therefore, will make a smaller angle with the shore than that by the boom as is depicted in Figure 2.

Figure 21c and d show the magnitude and direction of the drag on booms of different fin lengths. It is seen from Figure 21c that the drag on the boom increases as the fin length is increased. At the optimal boom position, the increase in D_* again is more or less proportional to the increase in L_f/L_b. Comparing to the curves in Figure 21a, one sees that the curves in Figure 21c are close to each other and D_* is small at large fin angle, meaning that increasing the fin length does not significantly increase the drag on the boom at its initial deployment position. This is desirable because the initial deployment of the boom will not become more difficult because of the increase of the length of the fins.

The curves on Figure 21d are similar to those on Figure 21b except that they are very close to each other, especially the part below the α axis. Thus, one sees that what has been discussed of Figure 21b will be equally valid for Figure 21d. The closeness of the curves at large fin angles means that the direction of the drag is insensitive to the length of the fin at large fin angles.

Based on Figure 21, once the flow velocity and the dimensions of the ice-oil boom are known, one may design the anchoring structure or mechanism on the shore.

3.0 LABORATORY EXPERIMENT

After thoroughly studying the dynamic performance of the ice-oil boom in the preceding part, the theoretical predictions should be verified by laboratory experiments and the necessary design coefficients should also be obtained from the laboratory. However, because of the timing of funding, it was necessary to limit the laboratory testing to preliminary and proceed with the design of the field prototype boom based on the preliminary laboratory testing and theoretical conclusions.

The more comprehensive laboratory study of the ice-oil boom has been planned and will be conducted in the next few months. Detailed results of the laboratory study will be reported in due time. Within the scope of this paper, however, only the preliminary laboratory experiment is reported.

For the preliminary laboratory study, three model boom sections of the shape and dimensions as shown in Figure 22 were constructed. The gap between the fin and the boom could be adjusted by sliding the fin along the hinged wires. The 45° openings were used to facilitate the deployment of the boom either from the right bank or the left bank of the flow by simply flipping it over. The fin angle was adjusted individually by the length of the string that tied the fin to the boom. The three sections of boom were flexibly connected with fishing tackles and were towed in a towing tank. Plastic chips and wooden blocks 10 cm x 10 cm x 5 cm (4"X4"X2") were placed in the towing tank before each run to simulate spilled oil and ice blocks respectively. For a few runs, large ice sheets measuring up to 1.2 m x 1.2 m x 2.5 cm (4'X4'X1") thick were used. Photographs and movies were taken to record the experiments. Figure 23 is a photograph showing the laboratory experiment.

The laboratory experiments showed that when being towed and with a fin angle of about 90°, the boom as a whole would make an angle of about 40° with the direction of tow. However, the angles made by the three individual boom sections were different. For the upstream section, the angle was the smallest at about 35° and for the last section, the angle was the largest at about 45°. An arch thus was formed by the three sections and the arch hindered the free movement of the simulated ice and oil. The arch was greatly reduced when the second last fin was removed. Under such a situation, the simulated oil flowed through the openings nicely and the boom smoothly guided the simulated ice blocks to one side. However, when the boom was hit by a large ice pane, it would

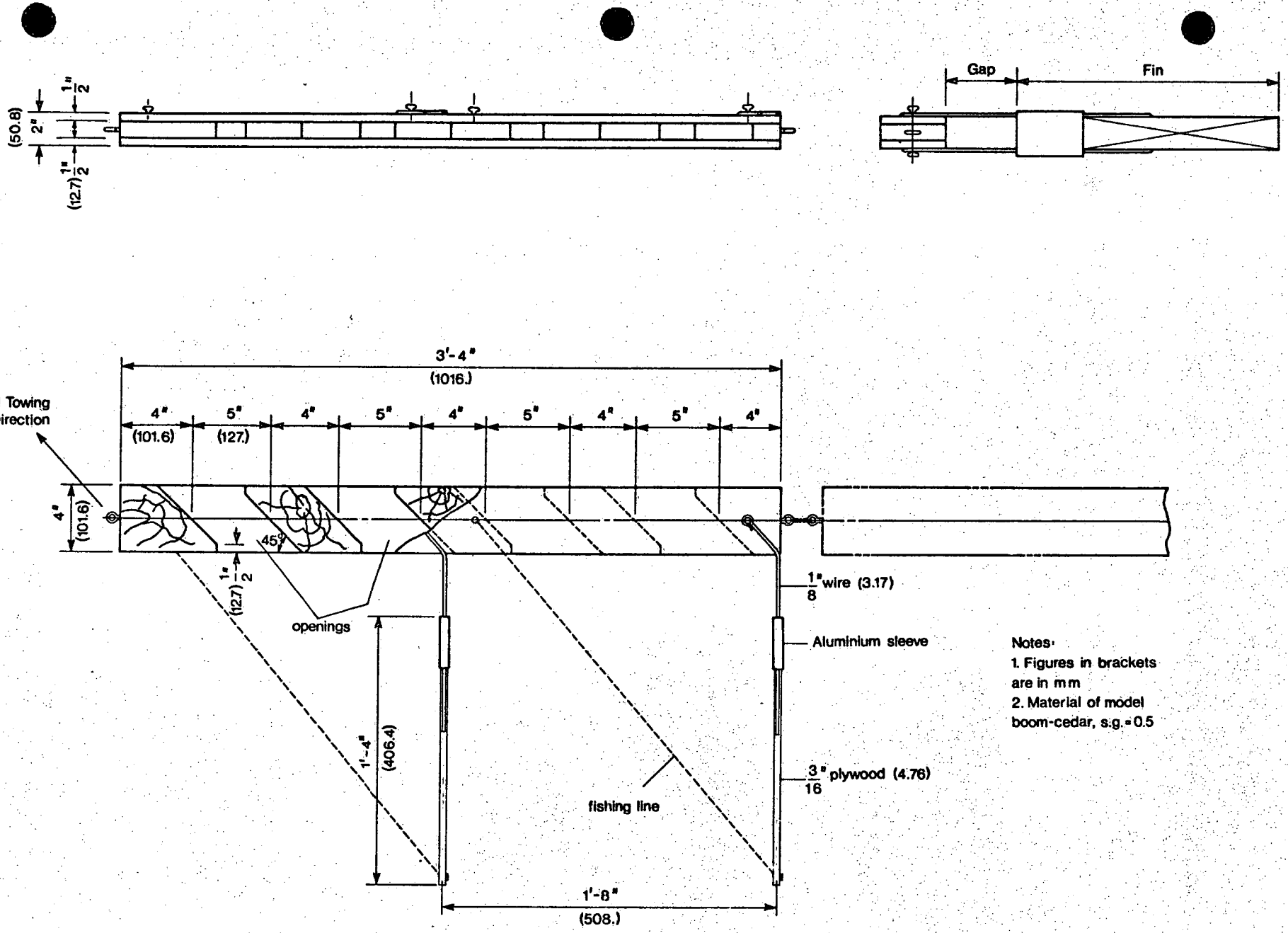

Fig 22 Model boom sections used in laboratory experiments

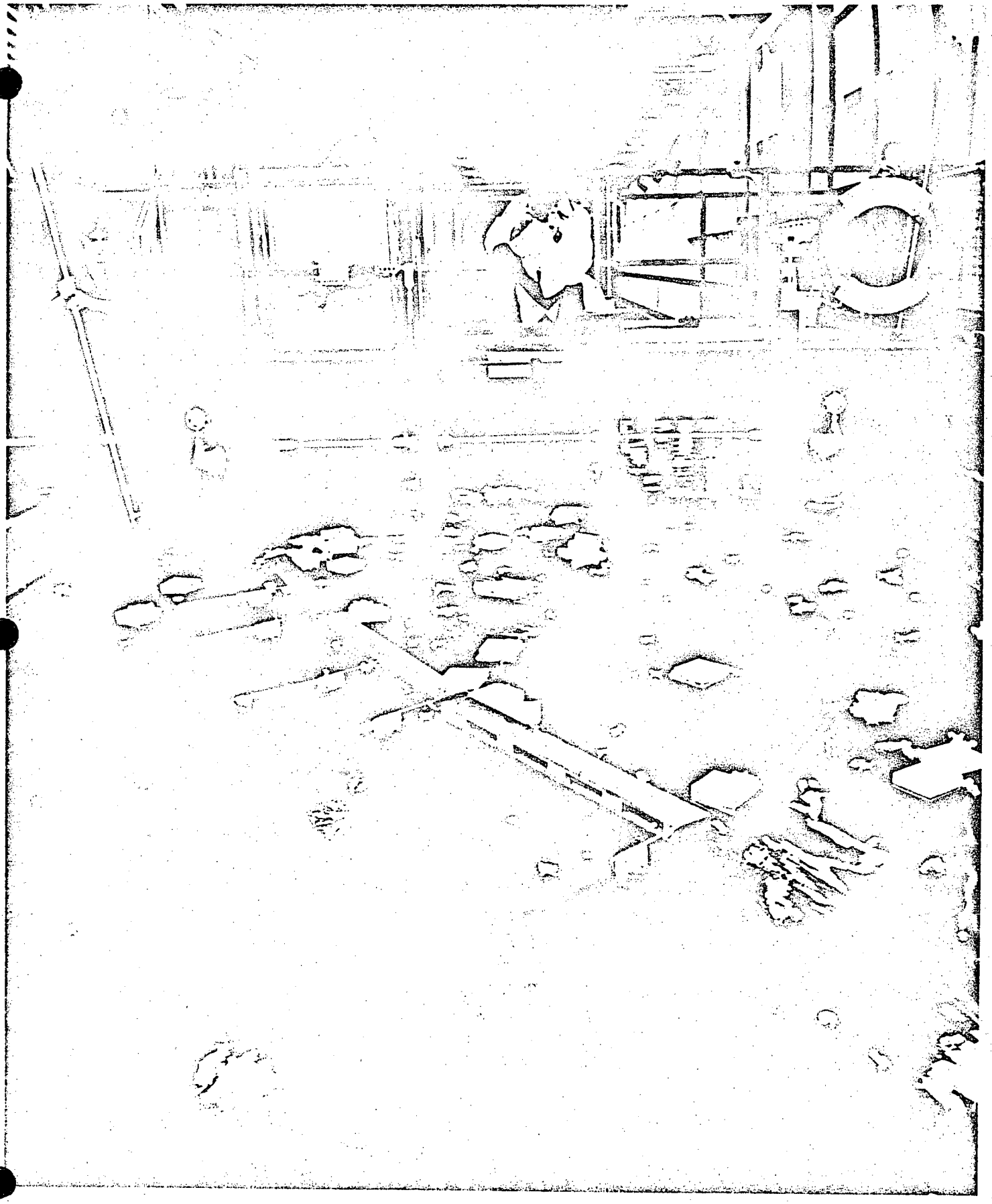

Fig. 23 Laboratory experiment of model boom in towing tank

deform to a certain degree and cause the ice pane to be caught between two boom sections for a short time. The total swinging of the boom, as a consequence of being hit by the ice pane, was observed to be small compared to the original boom angle of about 40^{o}. No attempt was made to test the boom with the sections rigidly connected. The tests were repeated at different towing speeds and the speed did not appear to affect the behaviour of the boom. For all the experiments, the fin gap width was roughly maintained at $L_g/L_b=0.25$.

From the preliminary laboratory experiments, the feasibility of the proposed ice-oil boom was confirmed and decision was made to proceed with the design, construction and field test of a prototype boom.

4.0 FIELD EXPERIMENT

4.1 Design and Construction of Prototype Boom

Based on theoretical investigations and the preliminary laboratory testing, a prototype boom as shown in Figure 24 was designed. It is seen from Figure 24 that each boom section consisted of two units of 3.05 m (10 feet) long each. A total of six sections were constructed giving a total boom length of 36.59 m (120 feet). In Figure 24, the dimensions shown on the lines were the design dimensions and the figures shown in brackets were the dimensions of the boom sections as constructed.

Hard wood was inadvertently used to construct the boom instead of the specified cedar. The heavy wood used, plus the construction discrepancy, caused the openings in the boom to be submerged below the water surface. To alleviate the problem, two inch thick styrofoam slabs were nailed to the bottom of the boom. The styrofoam lifted the openings out of submergency for about 4 cm (1½") but made the boom unstable and tilting. The stability was greatly improved when the fins were extended out to provide the balance force.

4.2 Field Test of Boom

The boom was tested in the Detroit River at Amhurstburg, Ontario in March 1978. Figure 25 shows the test site and the experimental layout. The surface velocity of the flow along I-I and II-II was measured with a current meter. The velocity measurement data are shown in Table 3. Because the measurements were made from a boat, a $\pm$10 percent error range appeared to be reasonable. The velocity distributions along I-I and II-II were also plotted on Figure 25. As a whole, one can see from Table 3 and Figure 25 that the average surface velocity at the site was about 0.55 m/s (1.8 ft/s).

Before the exercise, the boom sections and the fins were stacked up beside the bay. With a crew of four and the use of a mobile crane, a section could be fitted with the fins and placed in water in about 15 minutes and another half an hour was needed to cable the boom section and the fins. With better engineering design and an improved procedure, the deployment time can be greatly reduced. After the boom was assembled, it was towed by tug from the bay into the Detroit River and tied to a bollard on the pier for testing.

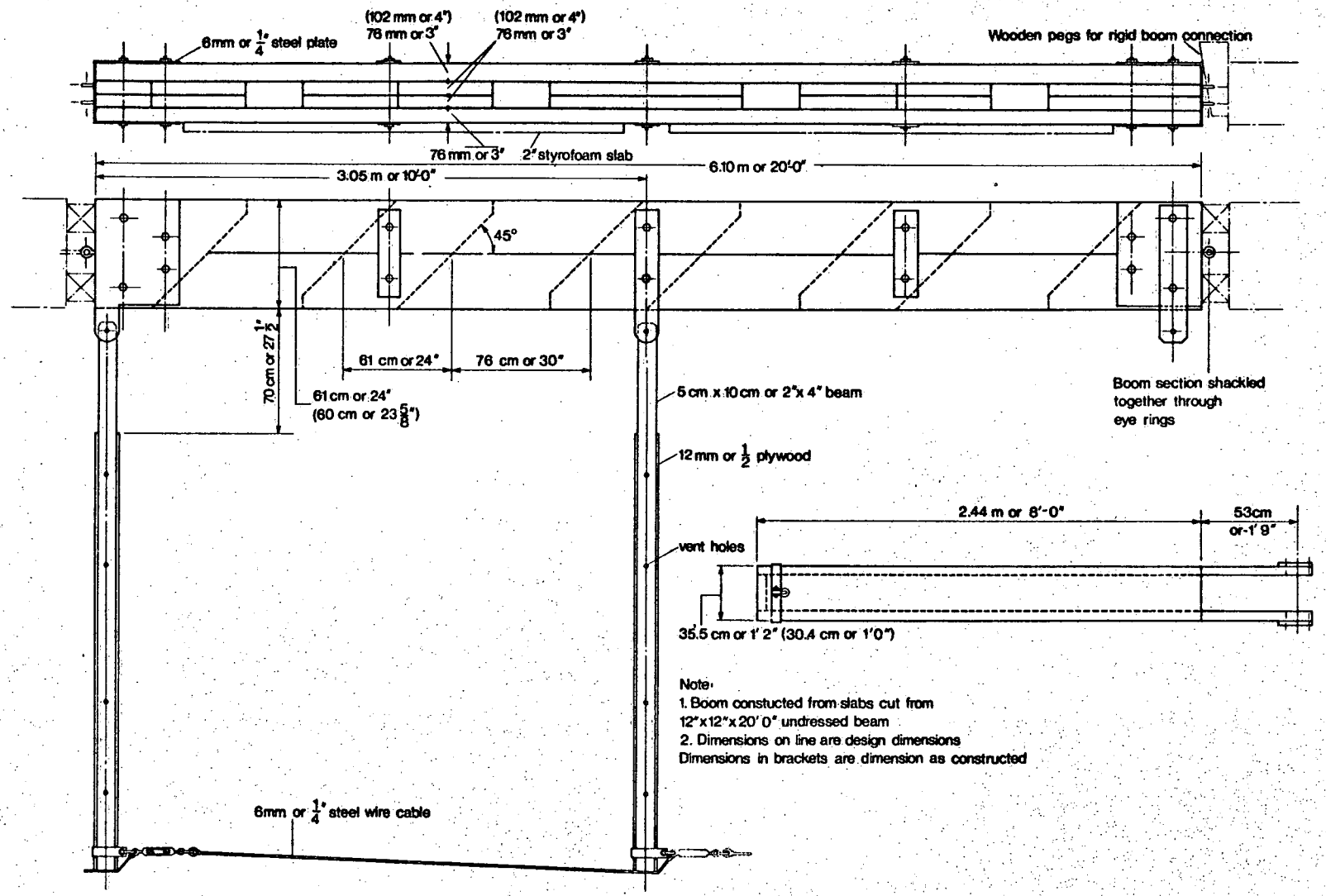

Fig24 Prototype Boom for Field Test

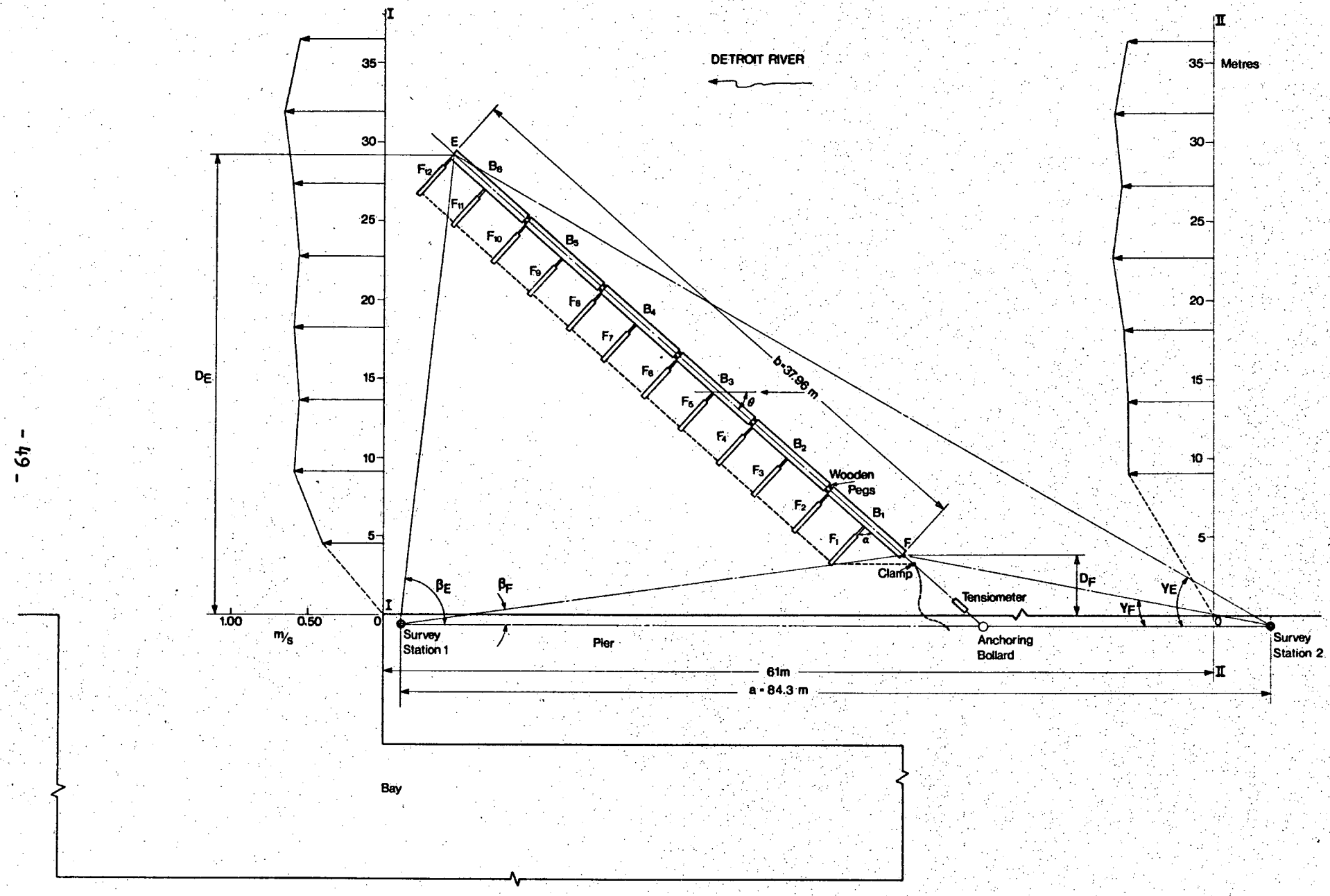

Fig 25 Experimental layout for Field Testing of Ice Oil Boom

TABLE 3 SURFACE VELOCITY OF CURRENT AT TEST SITE

Distance from Shore		Velocity Along I-I		Velocity Along II-II	
m	ft	m/s	ft/s	m/s	ft/s
4.57	15.0	0.40	1.3	-	-
9.15	30.0	0.58	1.9	0.55	1.8
13.72	45.0	0.55	1.8	0.55	1.8
18.29	60.0	0.58	1.9	0.58	1.9
22.87	75.0	0.55	1.8	0.64	2.1
27.44	90.0	0.58	1.9	0.58	1.9
32.01	105.0	0.64	2.1	0.64	2.1
36.59	120.0	0.55	1.8	0.55	1.8

Limited testing was first conducted on the flexibly connected boom. It quickly became evident that a flexible boom would deform excessively when hit by ice floes of relatively large size. The testing, therefore, was concentrated on the rigidly connected boom. The boom was made rigid by hammering wooden pegs between the boom sections. The boom was very stable under working conditions, even when hit by large ice floes, so the inserting of wooden pegs was done after the boom was deployed.

During the experiment, the fin angles were measured with a protractor by a team member working on the boom. Another team member measured the surface current velocity at the midpoints of each boom. Two methods were used to measure the boom angles. The first method was to measure the distances from the shore to the upstream and downstream ends of the boom with strings, as simultaneously as practicable, and then calculate the boom angle by trigonometry. The second method was to measure the angles between the baseline and the line of sight to the upstream end and downstream end of the boom from the two survey stations shown in Figure 25 and then calculate the boom angle analytically.

To measure the total force on the boom, both the boom cable and the fin cable were connected to a tension gauge as shown in Figure 25. The fin angle was changed by pulling the fin cable by hand by two men.

No attempt was made to record exactly the size of the ice floes and the yielding angles of the boom when it was hit by the ice floes. However, during the test period when measurements were made, ice floes as large as 20 m x 20 m x 0.2 m thick 70 ft x 70 ft x 8 in) by visual estimation have been encountered and the measured boom angles should reflect the working of the boom under such conditions. Figure 26 is a picture showing the boom under test conditions and a common large ice floe that drifted regularly down the river.

To study the passing of oil slick through the openings and the deflection of oil by the fins to the shore, plastic oil simulant was released upstream of the boom from a tug. Figures 27 and 28 are two pictures showing the oil simulant testing. Figure 27 shows the passing of the oil simulant through the openings and the simultaneous deflection of an ice floe by the boom. Figure 28 shows the conveyancy of the oil simulant by the deflected surface current by the fins towards the shore. Observations showed that only the oil simulant caught between ice floes could not pass through the openings. This was remarkable considering that the openings were not properly positioned due to construction errors. The observations also showed that the deflected current had no problem in carrying the oil simulant over more than 30 m (100 ft) to the shore.

4.3 Experimental Results and their Comparison with Theoretical Predictions

A total of 14 tests were conducted. The experimental results are tabulated in Table 4.

From Table 4 one sees that the presence of the boom in the flow did not significantly reduce the flow velocity, although it might have changed its direction. The velocity was measured with a Price current meter which is non-directional.

From Table 4 one also sees that the connection of all fins by a single cable gave room to the accumulation of error of the fin angle. For the tested range of fin angles, more than 10° difference in fin angle between different fins were not uncommon. This pointed to the direction either the fins should be maneuvered individually or only a few of them should be connected and maneuvered as a group.

The boom angles measured with theodolites and the boom angles measured with string lengths under similar conditions were quite close, as shown in Table 4. This means that in future studies, either way may be used depending on experimental particulars.

Fig. 26 Testing of Prototype boom in Detroit River

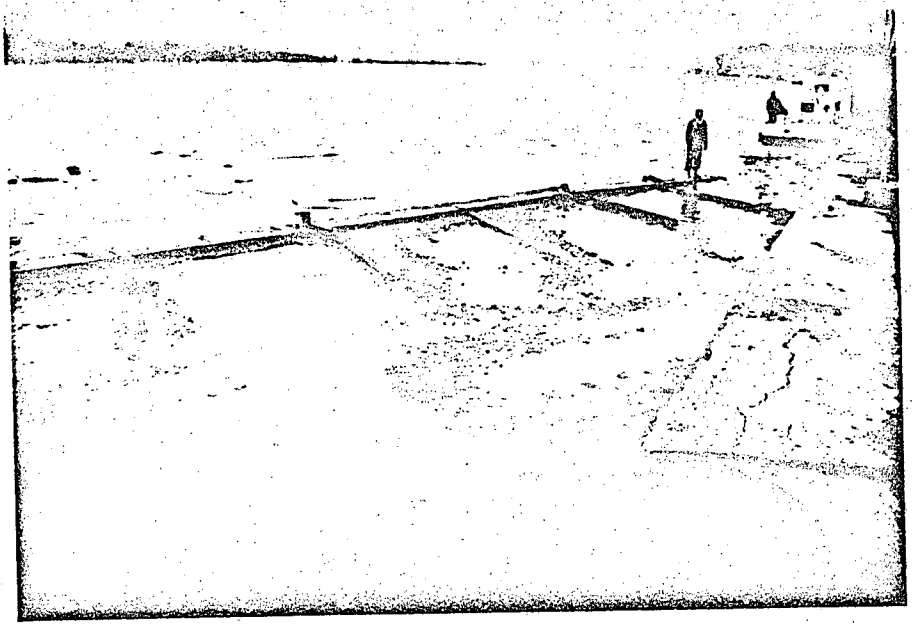

Fig 27 Passing of oil through boom and simultaneous deflection of ice floe

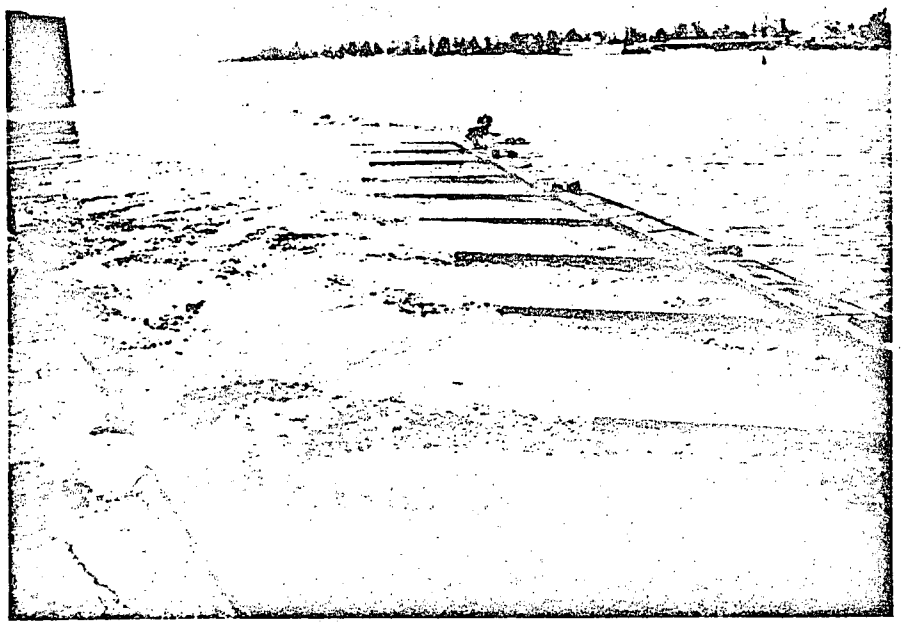

Fig 28 Deflection of oil to the shore by the fins

TABLE 4 RESULTS OF FIELD EXPERIMENT

Test No.	Fin Angle α, degrees													Surface Velocity of Current V*, m/s							Boom Angle θ, degrees	
	f_1	f_2	f_3	f_4	f_5	f_6	f_7	f_8	f_9	f_{10}	f_{11}	f_{12}	Avg.	B_1	B_2	B_4	B_4	B_5	B_6	Avg.	By Survey	By string lengths msmt.
1	78**	78**	76	76	76	78	81	81	82	85	88	90	81.3	0.46	0.58	0.58	0.46	0.43	0.46	0.49	0.5	-
2	-	-	92	93	92	92	97	96	101	93	96	96	94.8	0.36	0.37	0.52	0.58	0.64	0.55	0.50	15.4	-
3	105	106	109	111	111	112	116	117	113	112	119	120	112.5	0.40	0.43	0.55	0.46	0.46	0.58	0.48	26.5	-
4	107	107	111	111	111	111	113	110	109	109	107	114	110.0	0.43	0.67	0.58	0.58	0.46	0.58	0.54	24.3	-
5	89	91	92	93	96	96	99	99	98	98	100	100	95.9	0.27	0.46	0.43	0.52	0.58	0.52	0.46	16.0	16.1
6	92	92	96	97	99	99	102	102	102	101	102	102	98.8	0.46	0.43	0.64	0.64	0.58	0.64	0.56	17.8	17.6
7	101	101	101	99	101	101	101	101	101	100	103	102	101.0	0.46	0.52	0.58	0.67	0.64	0.64	0.59	18.0	20.1
8	96	98	101	102	102	104	105	105	104	104	104	106	102.6	0.46	0.52	0.55	0.55	0.64	0.64	0.56	18.3	19.7
9	99	101	103	103	105	105	108	107	106	106	108	107	104.8	0.40	0.46	0.55	0.58	0.64	0.58	0.53	17.8	19.8*;17.6*
10	109	109	111	111	111	111	115	115	112	112	115	115	112.2	0.52	0.43	0.58	0.58	0.58	0.67	0.56	19.1	17.7
11	116	118	120	118	118	118	120	118	118	118	118	118	118.2	0.40	0.55	0.52	0.67	0.64	0.64	0.57	25.0	26.4
12	127	127	127	127	127	127	128	128	125	124	124	125	126.3	0.46	0.58	0.52	0.46	0.55	0.58	0.52	16.1	16.9
13	134	-	132	-	132	-	134	-	128	-	127	-	131.2	0.46	0.52	0.52	0.43	0.64	0.64	0.53	21.1	19.6
14	-	148	147	146	144	141	141	140	134	133	134	133	140.0	0.52	0.52	0.46	0.43	0.58	0.58	0.52	22.4	22.7

Notes:

1. See Figure 25 for order of boom sections and fins.
2. Velocity was measured at midpoint of boom section
3. Boom angle by string length measurement is calculated from $\sin\theta=(D_E-D_F)/b$ (see Figure 25).
4. Boom angle by survey was calculated from (See Figure 25).

$$\sin\theta = \frac{a}{b}\left[\frac{\sin\beta_E \sin\gamma_E}{\sin(\beta_E+\gamma_E)} - \frac{\sin\beta_F \sin\gamma_F}{\sin(\beta_F+\gamma_F)}\right]$$

5. During the experiment, the wind was from S-SW at 7 knots. Ice was in the form of low density ice floes (i.e as discrete floes).
6. Thickness of ice: Large floes - 15-20 cm; Small floes - 8-10 cm; occasionally 30 cm.

* Under different ice conditions

** Fins touching shore

According to Table 4, the boom angle θ was plotted against the fin angle α for the tested boom as shown in Figure 29. In Figure 29, the theoretical θ-α curve for the prototype boom was also plotted. The parameters of the prototype boom, based on the actual construction dimensions, were $L_u/L_b=0$, N=12, $L_g/L_b=0.33$, $A_f/A_b=0.6$ and $L_f/L_b=0.8$. It may be pointed out that according to theoretical derivations L_g is defined as the distance from the upstream edge of the fin to the centre line of the boom and not as the gap length between the boom and the fin. In Figure 29, two enveloping curves containing the data points were also drawn.

It is seen from Figure 29 that within the reasonably expected experimental error range, the field experiment supported the theoretical predictions. The data points scatter closely about the theoretical curve and the two enveloping curves are of similar shape to the theoretical curve.

Should everything come nicely together, the upper enveloping curve should be more or less coincident with the theoretical curve. However, this is not the case and from Figure 29 one sees that the upper enveloping curve in places is up to 5^o above the theoretical curve. The θ_{max} values of the two curves are different by about 3.5^o. Two things could have caused the above. The first was that because of the tilting of the boom as a consequence of nailing styrofoam to the bottom of the boom, the fins were immersed in water more than that in the case when the boom floated squarely on the water. A greater drag, therefore, was exerted by the flow to the fins than otherwise to cause the boom to swing more into the flow. The second reason was that because the openings in the boom were chamferred, the flow through them would have met less resistance than when it encountered the fins. In other words, the drag coefficient for the boom body should be less than that for the fins. A greater drag coefficient for the fins than for the boom means that the boom would swing more into the flow.

Considering the upper enveloping curve approximately as the ice free curve of the prototype boom, from Figure 29, one sees that the maximum yield angle of the boom during the experiment was about 9.5^o. Presumably this maximum yield angle took place when the boom was hit by the largest ice floe of 20 m x 20 m x 0.2 m.

The theoretical relationship between the yield angle and the floe size for the prototype boom was calculated and plotted as shown in Figure 30. It is seen from Figure 29 that with a yield angle of 9.5^o the non-dimensional size of the ice floe that may be deflected is $V_{i*}=17$.

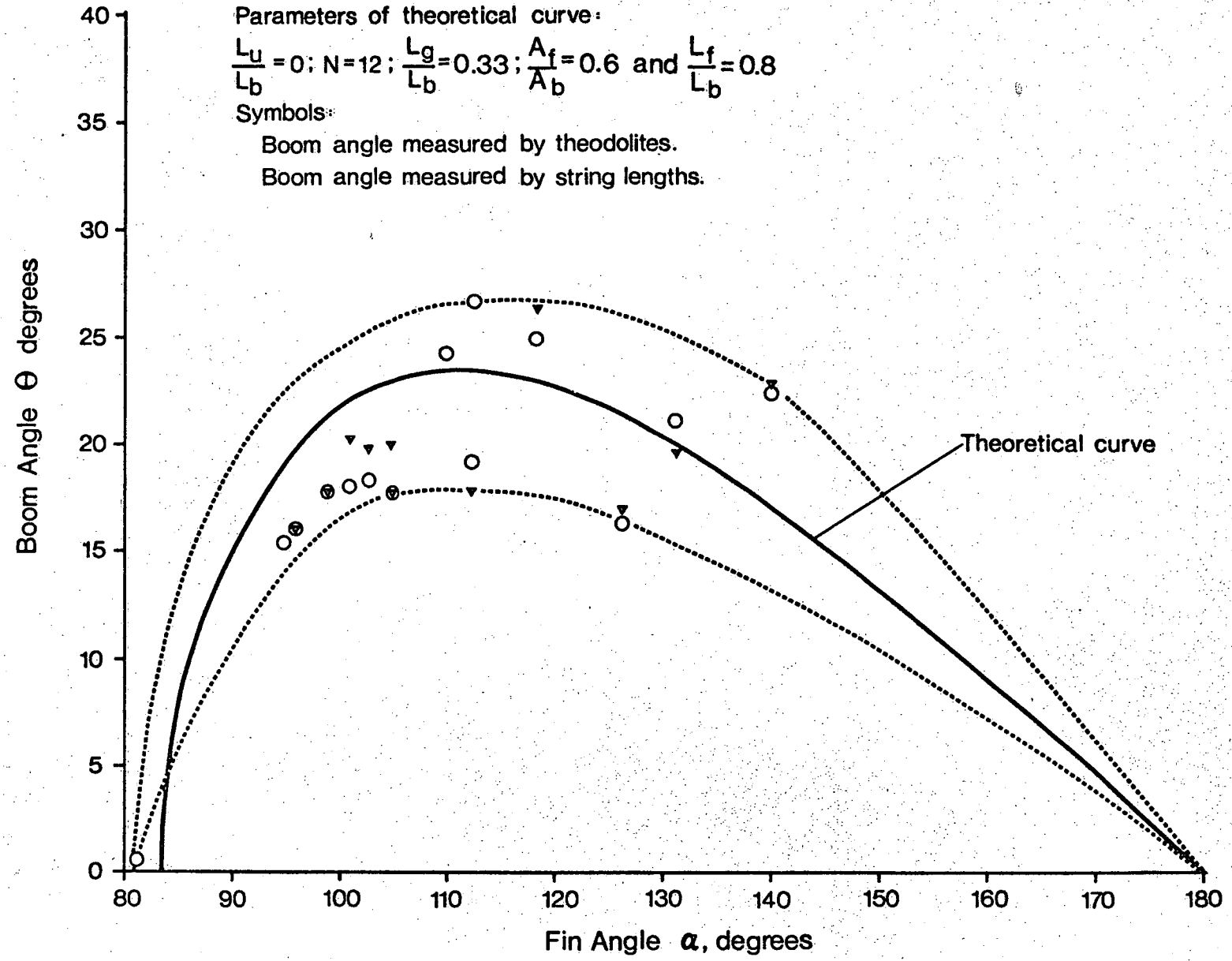

Fig29 Comparison of Θ-2 relationship between experimental results and theoretical predictions.

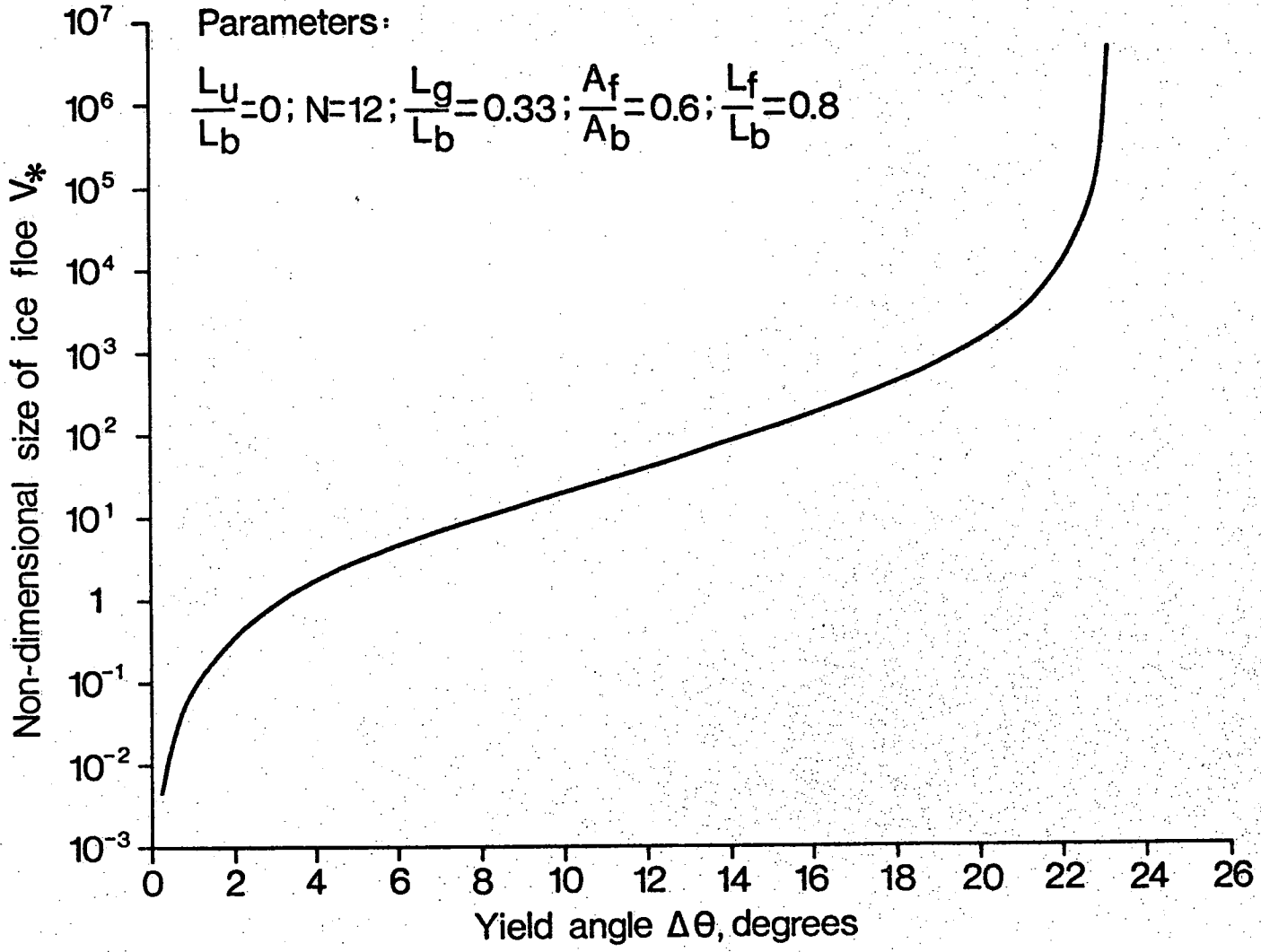

Fig30 Theoretical relationship between deflected floe size and yield angle for the prototype boom

Knowing V_{i_*}, the size of the ice floe can be calculated from the definition of V_{i_*} (see Equation 28)

$$V_{i_*} = \frac{1}{K} \frac{A_i t_i}{L_b^2 H_b} \tag{36}$$

K in the above equation is defined as

$$K = \frac{\rho C_D}{\rho_i \eta} \tag{37}$$

While the exact values of the drag coefficient C_D and the coefficient of virtual mass η have yet to be evaluated from experiments planned for the near future, as an approximation, they are given the value of 2 and this leads to a K value of about unity. Using this K value and the values of t_i=20 cm, H_b=23 cm and L_b=3.05 m based on the field experiment, a floe size of 13.5 m x 13.5 m x 0.2 m is calculated, which is comparable to the largest observed floe size of 20 m x 20 m x 0.2 m estimated visually.

Although a tensiometer was connected to the boom in the field experiment intending to measure the drag force, unfortunately, it malfunctioned and failed to measure the force. However, from manipulating the boom, it was found that three men together could pull the boom and two men together could adjust the fins.

5.0 CONCLUSIONS

Detailed theoretical study was made on the proposed ice oil boom. Guided by the theory, preliminary laboratory experiments were performed. Based on the theory and the preliminary laboratory study, a prototype boom was constructed and field tested. The study demonstrated that an ice-oil boom can be built for satisfactory deployment on flowing water infested with ice floes for oil spill containment and recovery.

Further work is being conducted both in the laboratory and in the field to obtain the necessary design coefficients, to improve the design, deployment and perforamcne of the boom, and to further compare the experimental results with theoretical predictions.

ACKNOWLEDGEMENT

This project would not have been possible without the cooperation and support received from many individuals and organizations. Special gratitude is due to the following persons and organizations they worked with: Mr. R. Carson of Hydraulics Research Division, NWRI, CCIW, for designing the prototype boom and assisting the laboratory testing; Cmdr. C. Corbett, USCG, for obtaining the funding and managing the contract for contracting the prototype boom; J. Bennett, CCG, for supervising the field test; Capt. C. Beckett, CCG, for assisting in organizing the field program and Drs. T. M. Dick and Y. L. Lau both of Hydraulics Research Division, NWRI, CCIW, for reviewing the report and making management contributions during the project.

REFERENCES

1. Brodsky, L., M. E. Charles, G. D. Greene and D. Mackay, 1977. The Use of Deflectors for the Deployment of Oil Booms at an Angle to River Currents". Petroleum Association for Conservation of the Canadian Environment, PACE Report No. 77-3.
2. Eryuzlu, N. E. and R. Hausser. "Use of Floating Deflector for Oil Spill Control in Fast Flowing Waters". Proceedings of the 1977 Oil Spill Conference, New Orleans, pp. 335-340.
3. Foley, J. P. and S. J. Tressidder, 1977. "The St. Lawrence River Oil Spill of June 23, 1976 - Are You Ever Truly Ready". Proceedings of the 1977 Oil Spill Conference, New Orleans, pp. 81-86.
4. Koroleff, A., 1932. "Glance Booms". Canadian Pulp and Paper Association, Woodland Section, Index No. 261 (B-9-e) pp. 1-11.
5. Lamb, H., 1932. "Hydrodynamics, 6th Edition, Cambridge University Press, pp. 76-77.
6. Lazier, S. S., 1964. "The Water Transport of Pulp Wood". Canadian Pulp and Paper Association, Woodland Section, Index No. 2297 (B-9-a), pp. 1-4.
7. Tsang, G., 1975. "Ice Conditions and the Proposed Containment and Removal of Spilled Oil on the St. Clair and Detroit Rivers". Scientific Series No. 56, Inland Waters Directorate, Environment Canada.
8. Vanderkooy, N., A. Robertson and C. J. Beckett, 1976. "Evaluation of Oil Spill Barriers and Deployment Techniques for the St. Clair-Detroit River System". Technology Development Report, EPS-4-EC-76-r, Environmental Protection Service, Environment Canada.